

The Timescales of Quantum Breaking

Marco Michel,^a Sebastian Zell^b

^a*Department of Physics, Ben-Gurion University of the Negev, Beer-Sheva 84105, Israel*

^b*Centre for Cosmology, Particle Physics and Phenomenology – CP3, Université catholique de Louvain, B-1348 Louvain-la-Neuve, Belgium*

E-mail: michelma@post.bgu.ac.il, sebastian.zell@uclouvain.be

ABSTRACT: Due to the inevitable existence of quantum effects, a classical description generically breaks down after a finite quantum break-time t_q . We aim to find criteria for determining t_q . To this end, we construct a new prototype model that features numerous dynamically accessible quantum modes. Using explicit numerical time evolution, we establish how t_q depends on the parameters of the system such as its particle number N . The presence of a classical instability leads to $t_q \sim \ln N$ or $t_q \sim \sqrt{N}$. In the stable case, we observe $t_q \sim N$, although full quantum breaking may not take place at all. We find that the different regimes merge smoothly with $t_q \sim N^\gamma$ ($0 < \gamma < 1$). As an outlook, we point out possibilities for transferring our results to black holes and expanding spacetimes.

Contents

1	Breakdown of the classical description	2
1.1	Computing the quantum break-time	2
1.2	Analogue models for gravity	5
2	Review of attractive one-dimensional Bose gas	6
2.1	Full model	6
2.2	Undercritical regime	8
2.3	Overcritical regime	10
2.4	Critical regime	11
2.5	Truncation	12
3	New prototype model	12
3.1	Extension by species	12
3.2	Undercritical regime	14
3.3	Overcritical regime	15
3.4	Critical regime	17
4	Numerical study	17
4.1	Comparison of prototype model and periodic system	17
4.2	Undercritical regime	18
4.3	Overcritical regime with few species	23
4.4	Overcritical regime with many species	26
4.5	Critical interpolation	29
5	Conclusion	33
5.1	Summary of findings	33
5.2	Outlook: connection to gravity	34
A	Bound on self-coupling	35
B	Undercritical regime	38
C	Overcritical regime with few species	40
D	Overcritical regime with many species	41
E	Critical interpolation	43

1 Breakdown of the classical description

1.1 Computing the quantum break-time

A fundamental description of our world must include quantum effects. Nevertheless, classical theories yield highly accurate results in many situations. Why this is the case and how localized wave functions correspond to classical trajectories have been important questions since the early days of quantum mechanics [1–8].¹ In particular, the classical solution is exact in special circumstances [8]. Generically, however, the classical description only has a limited range of applicability. Starting from a given initial state, the solution computed in the classical approximation cannot track indefinitely the expectation value derived from the true quantum evolution (see fig. 1). Following [10], we shall refer to the timescale t_q after which quantum effects invalidate the classical description as the *quantum break-time*.

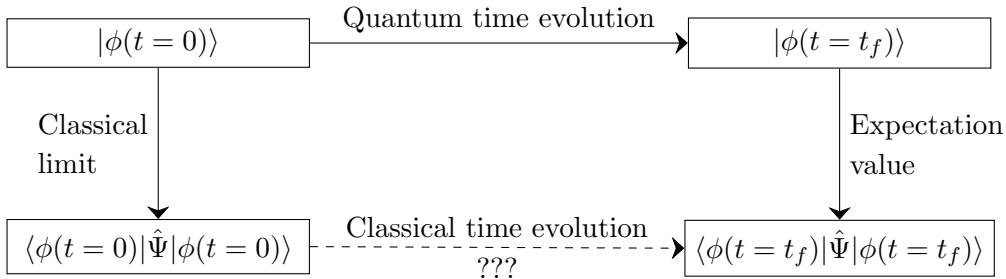


Figure 1: Schematic depiction of quantum breaking. Starting from an initial state $|\Phi(t = 0)\rangle$, exact dynamics corresponds to computing time evolution of the quantum state and then evaluating its expectation value. In the classical approximation, one already takes the expectation value of the initial state and then calculates time evolution classically. Quantum breaking occurs when these two approaches differ significantly.

An explicit study of t_q was first performed in small systems corresponding to a single quantum oscillator [11–13]. In certain situation, a fast quantum breaking was found, corresponding to the scaling [11, 12]²

$$t_q \sim \ln \hbar^{-1} , \tag{1.1}$$

where \hbar is the Planck constant. If the properties of the system are altered, the quantum break-time can also be much longer [12]:

$$t_q \sim \hbar^{-1} . \tag{1.2}$$

Finally, it was pointed out that also intermediate scalings are possible, [13, 17–19]:

$$t_q \sim \hbar^{-\gamma} , \tag{1.3}$$

¹See [9] for an English translation of [1].

²See [14–16] for further investigations leading to eq. (1.1).

where $0 < \gamma < 1$. The timescales (1.1) and (1.3) that are faster than linear emerge when an instability leads to chaotic behavior [20, 21].

Quantum effects can also play a crucial role in systems of many particles – famous examples are Bose-Einstein condensation [22, 23] and superconductivity [24, 25]. Nevertheless, one might expect that a classical approximation becomes increasingly accurate on macroscopic scales. Intriguing indications against this common belief come from gravity. As detailed below, a microscopic model of a black hole – the *quantum N -portrait* [26] – made evident that crucial deviations from the classical description can also occur for arbitrarily large objects [10, 27–30].

This sparked an interest in analogous phenomena in non-relativistic quantum many-body systems and a one-dimensional Bose gas with periodic boundary conditions [31, 32] was employed as prototype model. This system, to which we shall refer as *periodic prototype model (PPM)*, features an attractive contact interaction of strength α and exhibits two different regimes which are separated by a second order quantum phase transition [32] (see also [33–38]). The relevant control parameter is the collective coupling $\lambda = \alpha N$, where N is the particle number. One can normalize λ such that for $\lambda < 1$ the system is undercritical and the ground state is homogeneous while $\lambda > 1$ leads to overcriticality and a bright soliton. For $\lambda > 1$, the PPM exhibits quantum breaking on the timescale [10]

$$t_q \sim \frac{1}{\sqrt{\lambda - 1}} \ln N . \quad (1.4)$$

As in [20, 21], this logarithmic quantum break-time emerges due to an instability, where the prefactor in eq. (1.4) is set by the classical Lyapunov exponent [10].

Among various further studies [30, 39–48] about quantum effects in the PPM, an important question concerns the behavior of the system at the critical point $\lambda = 1$. In this case, there are indications that deviations from a classical description occur on the timescale [41]:

$$t_q \sim \sqrt{N} . \quad (1.5)$$

Finally, key findings about quantum breaking in the PPM continue to hold true in its relativistic generalization [49–53].

The PPM exhibits two peculiar phenomena. First, a recurrence takes place on short timescales for $\lambda > 1$: After quantum breaking has occurred, time evolution periodically returns to a state in which the classical approximation is again viable [10].³ It is reasonable to assume that this behavior is related to a smallness of the Hilbert space. Namely, only three quantum modes are relevant for the dynamics of the PPM if the collective coupling is not much bigger than its critical value, $\lambda \gtrsim 1$ [10]. A second open question arises from the fact that the undercritical regime, $\lambda < 1$, does not exhibit quantum breaking, i.e., the classical description remains a viable approximation indefinitely [48]. In contrast, various arguments

³Of course, a closed system will generically return close to its initial state but on much longer timescales [54, 55].

indicate that – at least in certain models – quantum breaking might also take place far away from a classical instability on the timescale [45, 48, 49, 56] (see also discussion in [57])

$$t_q \sim N . \tag{1.6}$$

Since an undercritical choice of parameters can certainly be regarded as more generic, it is important to determine if and under what conditions quantum breaking takes place without a classical instability.

A comment is in order regarding scrambling. This notion, which was also introduced in the context of black hole physics [58, 59], denotes a generation of entanglement such that information about the initial state can only be extracted by measurements involving a significant part of a quantum system. Clearly, the growth of such quantum correlations indicates a deviation from the classical description and indeed quantum breaking in the PPM can be regarded as a result of scrambling [10] (see also [46]).⁴ Studies of scrambling exist in a large variety of other systems; both logarithmic timescales $\sim \ln N$ [47, 61, 65–86] and polynomial scalings $\sim N^\gamma$ [57, 87–102] have been observed (see [103, 104] for recent reviews).

Finally, we briefly discuss the classical limit. It is evident from the dependencies (1.1), (1.2) and (1.3) that $\hbar \rightarrow 0$ leads to $t_q \rightarrow \infty$ and no quantum breaking occurs. Since dimensional analysis shows that $N \sim E/(\hbar\omega)$ (see [45, 49]), where E is the total energy and ω represents an elementary frequency of (free) oscillations, the classical limit corresponds to an infinite particle number, $N \rightarrow \infty$. Therefore, eqs. (1.4), (1.5) and (1.6) all imply $t_q \rightarrow \infty$ and the classical description stays valid indefinitely, as it should.

Goals & Outline of Results In the present work, our goal is to extend the above studies of quantum breaking in three steps:

1. Based on [10, 32], we shall develop a *new prototype model (NPM)* that features a variable number Q of dynamically accessible modes. In analogy to the PPM, the ground state is determined by a collective coupling λ . The regime $\lambda > 1$ can lead to the logarithmic quantum break-time (1.4), but the enlarged Hilbert space of the NPM ensures that recurrence is avoided, i.e., the system does not return to the initial classical state on short timescales. Moreover, a large Q causes a breakdown of the classical description in the regime $\lambda < 1$, corresponding to the absence of a classical instability, on the linear timescale (1.6). As to be discussed, however, such a big number of species puts into question the meaning of quantum breaking [105–107].
2. We will study how the quantum break-time depends on the various parameters of the NPM. In particular, we shall identify parts of parameter space in which $\lambda > 1$ leads to

⁴However, these two phenomena are not fully equivalent. For example, in certain situations a breakdown of the classical description may occur due to a loss of entanglement [60, 61]. Conversely, quantum breaking can be caused by memory burden instead if entanglement [62–64].

a classical instability but quantum breaking occurs on a polynomial timescale:⁵

$$t_q \sim N^\gamma, \quad (1.7)$$

where numerical fits indicate $\gamma \approx 1/2$.

3. We will interpolate between $\lambda < 1$ corresponding to $t_q \sim N$ and a parameter space in which $\lambda > 1$ and $t_q \sim \ln N$. This leads to a continuous transition and a quantum break-time given by eq. (1.7), where $0 < \gamma < 1$ depends smoothly on λ . Close to the critical point $\lambda \approx 1$, we observe $\gamma \approx 1/2$. This corresponds to the timescale (1.5), in analogy to the finding in the PPM [41].

The outline of the paper is as follows: After elaborating on the connection of quantum breaking and gravity in section 1.2, we will review the PPM of [32] and its features in section 2. Subsequently, we present in section 3 the NPM and derive analytic estimates related to the validity of the classical description. In section 4, we numerically compute real-time evolution to determine how the quantum break-time of the NPM depends on its different parameters, where we use the computer program *TimeEvolver* [108].⁶ In particular, we investigate how our system interpolates between the undercritical case $\lambda < 1$ and the overcritical regime of $\lambda > 1$. Finally, we conclude in section 5 and give an outlook to implications of our results for gravity.

1.2 Analogue models for gravity

As discussed above, an important motivation for studying quantum breaking originates from open questions related to black holes. Therefore, we shall give a brief review of selected issues in high-energy physics. Classically, black holes are stable and (in the absence of rotation) static, but once quantum effects are included they emit Hawking radiation [117]. The computation of [117] is semi-classical, i.e., quantum fields are studied in the background of a classical and fixed black hole metric. Nevertheless, it is clear that the produced particles must backreact on the black hole, not least because of energy conservation. However, how exactly the black hole evolves as a result of Hawking evaporation is an open question [118]. As one option, it is possible that its classical description breaks down once a sufficient number of particles has been emitted [119]. In particular, it appears that unitarity is violated if black hole evaporation can still be computed semi-classically after half of its mass is lost [120].

The purpose of the quantum N-portrait [26] is to address these issues in a microscopic model. In it a black hole of mass M and Schwarzschild radius $r_g = 2G_N M$ consists of $N = G_N M^2 / \hbar$ soft gravitons, where G_N is Newton's constant. These constituent gravitons have wavelength r_g and interact with coupling strength $\alpha = \hbar G_N / r_g^2 = 1/N$. Therefore, the collective coupling gives $\lambda = \alpha N = 1$ and quantum criticality appears as a crucial property of

⁵A possible sublinear polynomial scaling of the quantum break-time has also been pointed out in [63].

⁶*TimeEvolver* relies on Krylov-subspace methods for computing real-time dynamics. Similar techniques have e.g., recently also been employed in [93–95, 100, 109–115] (see discussion in [116]).

black holes [10, 26–29]. Studying the PPM close to the critical point $\lambda = 1$ yielded indications that the classical description of a black hole ceases to be valid at the latest after half of the mass is lost [28, 40, 41, 43]. In particular, such a finding ensures compatibility with unitary time evolution.

The PPM and the approach of [28] led to the development of new non-relativistic analogue systems that share important properties with black holes [62, 64, 121]. Whereas previous proposals focused on imitating geometry [122–126] (see [127, 128] for reviews), these new models reproduce information-theoretic characteristics of a black hole, in particular its Bekenstein-Hawking entropy [129]. Such an approach is especially useful for gathering information about the fate of a black hole after its half lifetime: Hints were found that black hole evaporation can slow down drastically once its classical description has broken down [64].

Related issues also arise in expanding spacetimes, especially in the de Sitter solution of General Relativity. Classically, this system is eternal but quantum effects also cause particle production [130], in close analogy to Hawking radiation. Again this leads to a question about how the generated particles backreact on the de Sitter spacetime [131–134]. As in the black hole case, this issue is also linked to unitarity [135–138]. Moreover, there are proposals for employing analogue quantum systems for studying quantum effects in an expanding Universe [139–144], where as in [122] the focus is on imitating geometric properties.

Similarly to the quantum N-portrait [26] of a black hole, one can develop a microscopic model of de Sitter and inflationary spacetimes [49, 56, 145–147]:⁷ Now the constituent gravitons have wavelength H^{-1} and their number is $N = 1/(\hbar G_N H^2)$, where H is the Hubble rate. Since the strength of gravitational interactions is given by $\alpha = \hbar G_N H^2$, again $\lambda = 1$ and criticality emerges as a crucial property. Moreover, the microscopic model strongly deviates from the description in terms of a classical metric once the backreaction of produced particles becomes sizable [49, 56]. These studies were developed further to include information-theoretic aspects, in particular the Gibbons-Hawking entropy [130] of de Sitter. As a result, hints emerged for the existence of new observables for inflation that are invisible in the semi-classical description and that are sensitive to the whole duration of inflationary expansion [63].

2 Review of attractive one-dimensional Bose gas

2.1 Full model

Following the analysis of [32], we shall review the model of an attractively interacting cold Bose gas on a 1- d circle. Its Hamiltonian is given by:⁸

$$\hat{H} = \frac{\hbar^2}{2mR^2} \int_0^{2\pi} d\theta \left[-\hat{\psi}^\dagger(\theta) \partial_\theta^2 \hat{\psi}(\theta) - \frac{\pi\alpha}{2} \hat{\psi}^\dagger(\theta) \hat{\psi}^\dagger(\theta) \hat{\psi}(\theta) \hat{\psi}(\theta) \right], \quad (2.1)$$

⁷See also [148] for an analogous approach for resolving classical backgrounds in QED.

⁸We choose $\hat{\psi}$ to be dimensionless such that $[\hat{\psi}(\theta), \hat{\psi}^\dagger(\theta')] = \delta(\theta - \theta')$.

where R is the radius of the circle, α a dimensionless coupling constant and m corresponds to the particle mass. Throughout this paper we will assume $\alpha > 0$. From here on, we shall choose units of energy such that $\hbar^2/(2mR^2) = 1$. In the mean field approximation, we split the (time-dependent) wave function in a classical contribution and fluctuations, $\hat{\psi}(t, \theta) = \psi_0(t, \theta) + \delta\hat{\psi}(t, \theta)$. The solution of the mean field is determined by the Gross-Pitaevskii equation:

$$i\hbar\partial_t\psi_0(t, \theta) = (-\partial_\theta^2 - \pi\alpha|\psi_0(t, \theta)|^2)\psi_0(t, \theta) = \mu\psi_0(t, \theta), \quad (2.2)$$

where μ is a Lagrange multiplier enforcing the constraint of particle number conservation, $\int_0^{2\pi} d\theta |\psi_0(t, \theta)|^2 = N$.

For periodic boundary conditions we can obtain two stationary solutions, $\psi_0(t, \theta) = e^{-i\mu t/\hbar}\psi_0(\theta)$, from eq. (2.2) [32, 149]. The first one is a homogeneous condensate,

$$\psi_0^{(<)}(\theta) = \sqrt{\frac{N}{2\pi}}. \quad (2.3)$$

The second one only exists for $\lambda > 1$ and corresponds to a bright soliton,

$$\psi_0^{(>)}(\theta) = \sqrt{\frac{NK(m)}{2\pi E(m)}} dn\left(\frac{K(m)}{\pi}(\theta - \theta_0)|m\right), \quad (2.4)$$

where $dn(u|m)$ is a Jacobian elliptic function and $K(m)$ as well as $E(m)$ correspond to the complete elliptic integrals of the first and the second kind, respectively. Finally, m is determined by the equation

$$K(m)E(m) = (\pi/2)^2\lambda, \quad (2.5)$$

and we introduced the collective coupling

$$\lambda = \alpha N. \quad (2.6)$$

For small $\lambda < 1$, the ground state is given by eq. (2.3). For large $\lambda > 1$, the homogeneous condensate (2.3) becomes unstable and the energy functional is minimized by the solution (2.4) with center θ_0 . Both phases are separated by a second order phase transition at $\lambda = 1$.

Rather than working in position space, it will be more convenient to go to momentum space. To this end, we expand the field operators $\hat{\psi}$ in Fourier modes

$$\hat{\psi}(\theta) = \frac{1}{\sqrt{2\pi}} \sum_{k=-\infty}^{\infty} \hat{a}_k e^{ik\theta}, \quad (2.7)$$

where the creation and annihilation operators \hat{a}_k^\dagger of (angular) momentum mode k satisfy the usual canonical commutation relations

$$[\hat{a}_j, \hat{a}_k^\dagger] = \delta_{kj}, \quad [\hat{a}_j, \hat{a}_k] = [\hat{a}_j^\dagger, \hat{a}_k^\dagger] = 0. \quad (2.8)$$

By plugging this expansion into the Hamiltonian (2.1), we arrive at:

$$\hat{H} = \sum_{k=-\infty}^{\infty} k^2 \hat{n}_k - \frac{\alpha}{4} \sum_{k,l,m=-\infty}^{\infty} \hat{a}_k^\dagger \hat{a}_l^\dagger \hat{a}_{m+k} \hat{a}_{l-m}. \quad (2.9)$$

In the present paper, a homogeneous condensate, i.e., a state in which only the \hat{a}_0 -mode is occupied,

$$|\text{in}\rangle = |N, 0, \dots, 0\rangle, \quad (2.10)$$

plays a special role and will be used as an initial state for time evolution. Throughout we will assume $N \gg 1$ so that we can employ the Bogoliubov approximation, $\hat{a}_0 \approx \sqrt{N}$, to get [28, 30]:

$$\hat{H} = \sum_{k \neq 0} \left(k^2 - \frac{\lambda}{2} \right) \hat{n}_k - \frac{\lambda}{4} \sum_{k \neq 0} \left(\hat{a}_k^\dagger \hat{a}_{-k}^\dagger + \hat{a}_k \hat{a}_{-k} \right). \quad (2.11)$$

In eq. (2.11), we neglected contributions of order \hat{a}_k^4 for $k \neq 0$. This leads to an error that scales like $1/N$.

The reason for the choice (2.10) of initial state is twofold. First, $|\text{in}\rangle$ corresponds to the mean-field solution (2.3), which is energetically favorable for $\lambda < 1$. Even though $|\text{in}\rangle$ has no connection to the ground state for $\lambda > 1$, its classical limit, corresponding to the homogeneous condensate (2.3), is still a mean field solution, albeit an unstable one. Therefore, it does not evolve in time, as long as no symmetry-breaking perturbations are included.⁹ Consequently, any time evolution away from the initial state inevitably leads to a deviation from classicality for all values of λ , as discussed in [10, 46, 47]. The second reason for choosing $|\text{in}\rangle$ is that one can make an inference from the occupation number of the \hat{a}_0 -mode to the full quantum state: A state is close to eq. (2.10) if and only if the occupation number of the \hat{a}_0 is close to N . As a result, evaluating the expectation value of \hat{n}_0 suffices for identifying quantum breaking.

2.2 Undercritical regime

For diagonalizing the system, we perform the Bogoliubov transformation [28, 30]

$$\hat{a}_k = u_k \hat{b}_k + v_k^* \hat{b}_{-k}^\dagger, \quad (2.12)$$

where we set

$$u_k^2 = \frac{1}{2} \left(\frac{k^2 - \frac{\lambda}{2}}{\epsilon_k} + 1 \right), \quad v_k^2 = \frac{1}{2} \left(\frac{k^2 - \frac{\lambda}{2}}{\epsilon_k} - 1 \right), \quad (2.13)$$

and defined

$$\epsilon_k = \sqrt{k^2 (k^2 - \lambda)}. \quad (2.14)$$

This yields

$$\hat{H} = \sum_{k \neq 0} \epsilon_k \hat{n}_k^b. \quad (2.15)$$

⁹The formation of the inhomogeneous soliton is discussed in [33, 34, 37, 38].

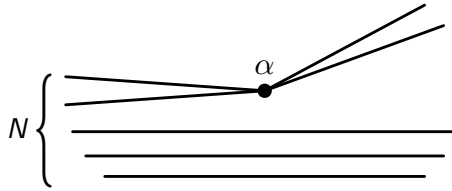


Figure 2: Schematic depiction of the leading-order process by which an initial state (on the left), in which particles are in the \hat{a}_0 -mode, evolves towards a state (on the right), in which two particles have left the \hat{a}_0 -mode.

Evidently, the Bogoliubov transformation defined by eq. (2.13) only exists in the undercritical case $\lambda < 1$. We shall first analyze the system in this parameter regime.

Our goal is to decide whether quantum breaking can take place in this case. To this end, we need to determine by how much time evolution can take the system away from the initial state (2.10). We can obtain an estimate by considering the ground state $|0_b\rangle$ of the Bogoliubov modes. Computing the number of depleted particles, i.e., particles that are not in the \hat{a}_0 -mode, yields

$$N_d = \sum_{k \neq 0} \langle 0_b | \hat{n}_k | 0_b \rangle = \sum_{k \neq 0} |v_k|^2 = \frac{1}{2} \sum_{k \neq 0} \left(\frac{k^2 - \frac{\lambda}{2}}{\sqrt{k^2(k^2 - \lambda)}} - 1 \right). \quad (2.16)$$

For $\lambda \ll 1$, we obtain [48]

$$N_d = \frac{\pi^4 \lambda^2}{720} \approx 0.135 \lambda^2. \quad (2.17)$$

We conclude that depletion is small, $N_d \ll 1 \ll N$, in the undercritical regime. We must emphasize, however, that time evolution in a closed system will never lead to the Bogoliubov ground state. Therefore, the number (2.17) can only be viewed as a qualitative estimate of the possible magnitude of deviations from the initial state (2.10). Nevertheless, eq. (2.17) clearly indicates that starting from the initial state (2.10), most particles will stay in the zero mode. Thus, time evolution will not lead to a large departure from the initial state and quantum breaking cannot take place. As a second inference from eq. (2.17), we observe that only the modes $k = \pm 1$ contribute significantly to depletion. If we only consider these two modes, we get

$$N_d^{(1)} = \frac{\lambda^2}{8} = 0.125 \lambda^2, \quad (2.18)$$

which is very close to the total number N_d of depleted particles.

Even though no significant departure from the initial state (2.10) will occur, we can estimate the speed at which particles leave the zero modes in the very first moments of time evolution. To this end, we consider a process in which two particles of the \hat{a}_0 -modes annihilate and produce two particles in a mode with non-zero k (see fig. 2). As is evident from eq. (2.9), the amplitude of such a process scales as α . This leads to the rate (see also [27–29, 49, 56])

$$\Gamma = N^2 \alpha^2 = \lambda^2, \quad (2.19)$$

where the enhancement of N^2 is due to the fact that in the state (2.10), there are approximately N^2 possibilities for choosing the two particles of the \hat{a}_0 -mode that annihilate. Generically, the rate (2.19) receives additional contributions with higher powers of λ . Thus, this formula is only valid if λ is sufficiently smaller than 1. If the process of generating particles with non-zero k were to continue – which it does not – with the rate (2.19), then we would be able to estimate the resulting quantum break-time. Namely, the number ΔN of particles that have departed the \hat{a}_0 -mode would be given as

$$\Delta N = \Gamma t . \quad (2.20)$$

This would result in the quantum break-time as the timescale when $\Delta N \sim N$:

$$t_q = N\Gamma^{-1} = \frac{N}{\lambda^2} . \quad (2.21)$$

We must reiterate, however, that the timescale (2.21) is fictitious since quantum breaking does not take place in the system (2.9) for $\lambda < 1$.

2.3 Overcritical regime

The Bogoliubov transformation employed in the previous section is only valid in the undercritical regime $\lambda < 1$. In order to study excitations in the overcritical case, we shall include perturbations in the Gross-Pitaevskii equation (2.2). To leading order in $\delta\hat{\psi}(t, \theta)$, we get [32]:

$$(-\partial_\theta^2 - 2\pi\alpha|\psi_0(t, \theta)|^2 - \mu) \delta\hat{\psi}(t, \theta) - \pi\alpha\psi_0^2(t, \theta)\delta\hat{\psi}^\dagger(t, \theta) = \omega_k\delta\hat{\psi}(t, \theta) , \quad (2.22)$$

$$(-\partial_\theta^2 - 2\pi\alpha|\psi_0(t, \theta)|^2 - \mu) \delta\hat{\psi}^\dagger(t, \theta) - \pi\alpha\psi_0^{\dagger 2}(t, \theta)\delta\hat{\psi}(t, \theta) = -\omega_k\delta\hat{\psi}^\dagger(t, \theta) , \quad (2.23)$$

where ω_k are the Bogoliubov-de Gennes frequencies [150, 151]. For the homogeneous solution (2.3), we have $|\psi_0|^2 = \sqrt{N}/\sqrt{2\pi}$ and correspondingly $\mu = -\alpha N/2$. Using the mode expansion (2.7) for $k \neq 0$, we arrive at [32] (see also [45])

$$\omega_k = \sqrt{k^2(k^2 - \lambda)} . \quad (2.24)$$

For $\lambda < 1$, this agrees with the result (2.14) of the Bogoliubov transformation. However, the result (2.24) is also valid in the overcritical regime, i.e., for $\lambda > 1$. In this case, the lowest-lying frequency becomes imaginary,

$$\omega_1 = i\sqrt{\lambda - 1} , \quad (2.25)$$

which signals the presence of an instability.

From this finding we can derive a rough estimate of the quantum break-time. In order to account for the instability, a contribution should appear in the depletion rate Γ that scales with the number ΔN of particles that have already left the \hat{a}_0 -mode. This effects should also depend on the magnitude of the imaginary frequency (2.25) and vanish for $\omega_1 \rightarrow 0$. Correspondingly, we modify the rate (2.19) as:

$$\Gamma = \lambda^2 + \sqrt{\lambda - 1}\Delta N , \quad (2.26)$$

where we employed a linear power of ω_1 , as also in [10]. Needless to say, this formula only represents a rough estimate and its implications remain to be verified. In particular, the derivation of the first term $\sim \lambda^2$ is only valid for $\lambda < 1$, but we expect that extrapolating is possible since the rate of perturbative scattering does not change qualitatively for $\lambda \gtrsim 1$. In any case, we are interested in the case when the second term in eq. (2.26) dominates. Then the number of depleted particles becomes

$$\Delta N = e^{\sqrt{\lambda-1}t}. \quad (2.27)$$

Consequently, $\Delta N \sim N$ leads to fast quantum breaking after the timescale [10] (cf. eq. (1.4))

$$t_q = \frac{\ln N}{\sqrt{\lambda-1}}. \quad (2.28)$$

As in the undercritical case, we will finally study the number N_d of particles that are outside the \hat{a}_0 -mode in the ground state. Since for $\lambda > 1$ the homogeneous state (2.10) is no longer related to the ground state (2.4), we expect this number to be macroscopic. Indeed, we can derive from eq. (2.7) in the mean-field approximation:

$$a_k = \frac{1}{\sqrt{2\pi}} \int d\theta e^{-ik\theta} \psi_0(\theta). \quad (2.29)$$

Whereas the homogeneous condensate (2.3) would lead to $a_k \sim \delta_{k0} \sqrt{N}$, the ground state for $\lambda > 1$ is given by the bright soliton (2.4). Thus, $a_k \sim \sqrt{N}$ at least for one $k \neq 0$ and we conclude that

$$N_d \sim N. \quad (2.30)$$

Even though the ground state can never be reached dynamically in a closed system, this indicates that quantum breaking generically takes place for $\lambda > 1$, in agreement with previous findings [10]. Starting from the initial state (2.10), we can estimate how many particles leave the \hat{a}_0 -mode. Namely, the instability disappears due to backreaction, i.e., that fact that particles leaving the \hat{a}_0 -mode effectively decrease the collective coupling λ (see also [32]). This yields

$$\sqrt{\lambda \left(1 - \frac{\Delta N}{N}\right)} = 1, \quad \Rightarrow \quad \Delta N = N \frac{\lambda - 1}{\lambda}. \quad (2.31)$$

2.4 Critical regime

At the critical point $\lambda = 1$, we can obtain an estimate for the number of depleted particles by extrapolating the result (2.16) of the undercritical regime. To this end, we take into account backreaction to derive from eq. (2.16):

$$N_d = \frac{1 - \frac{\lambda}{2} \left(1 - \frac{N_d}{N}\right)}{\sqrt{1 - \lambda \left(1 - \frac{N_d}{N}\right)}} - 1, \quad (2.32)$$

where we neglected all modes $|k| > 1$. This is possible since they are still undercritical at $\lambda = 1$ and so their contribution to depletion can still be estimated by eq. (2.17). For $N_d \ll N$, eq. (2.32) implies [32] (see also [42]):

$$N_d = \frac{N^{1/3}}{2^{2/3}} \left(1 + O\left(\frac{1}{N^{2/9}}\right) \right). \quad (2.33)$$

Analytic arguments relying on the limit of large N as well as numerical analysis indicate that the quantum break-time scales as [41]

$$t_q \sim \sqrt{N}. \quad (2.34)$$

2.5 Truncation

As is evident from the previous discussion, depletion is mostly due to the modes $k = \pm 1$ for all values of λ (as long as $\lambda < 4$). Therefore, we shall consider the truncation of the model (2.9) to three modes:

$$\hat{H} = \hat{n}_{-1} + \hat{n}_1 - \frac{\alpha}{4} \sum_{k,l=-1}^1 \sum_{m=\max(-k-1,l-1)}^{\min(-k+1,l+1)} \hat{a}_k^\dagger \hat{a}_l^\dagger \hat{a}_{m+k} \hat{a}_{l-m}. \quad (2.35)$$

The motivation to consider this system is simplicity or equivalently better suitability for numerical study. Since modes with $k \geq 2$ do not contribute significantly to quantum breaking, we can discard them from the outset.

In the case $\lambda < 1$, the truncation of Hamiltonian (2.11) after Bogoliubov approximation leads to

$$\hat{H} = \left(1 - \frac{\lambda}{2}\right) (\hat{n}_{-1} + \hat{n}_1) - \frac{\lambda}{2} (\hat{a}_1^\dagger \hat{a}_{-1}^\dagger + \hat{a}_1 \hat{a}_{-1}), \quad (2.36)$$

and the Bogoliubov Hamiltonian (2.15) becomes

$$\hat{H} = \sqrt{1 - \lambda} (\hat{n}_{-1}^b + \hat{n}_1^b). \quad (2.37)$$

For $\lambda \lesssim 1$, the number of depleted particles is still given by eq. (2.32), where we took into account backreaction. For $\lambda < 1$, the solution is

$$N_d = \left(\frac{1 - \frac{\lambda}{2}}{\sqrt{1 - \lambda}} - 1 \right) \left(1 - \frac{\lambda^2}{4(1 - \lambda)^{3/2}N} + O\left(\frac{1}{N^2}\right) \right). \quad (2.38)$$

In the critical and overcritical cases, the results (2.33) and (2.30) remain valid.

3 New prototype model

3.1 Extension by species

Now we shall consider a modified version of the model (2.35):¹⁰

$$\hat{H} = \hat{n}_1 - \frac{\alpha}{4} \left(2\hat{n}_0 \hat{n}_1 + \hat{a}_0^\dagger \hat{a}_1^2 + \hat{a}_1^\dagger \hat{a}_0^2 \right). \quad (3.1)$$

¹⁰A related simplification was considered in [121, 152, 153].

Again using the state (2.10), we get in the Bogoliubov approximation, $\hat{a}_0 \approx \sqrt{N}$,

$$\hat{H} = \left(1 - \frac{\lambda}{2}\right) \hat{n}_1 - \frac{\lambda}{4} \left(\hat{a}_1^2 + \hat{a}_1^{\dagger 2}\right), \quad (3.2)$$

where we used the collective coupling λ defined in eq. (2.6) and again neglected an error that scales as $1/N$. We already observe that eq. (3.2) resembles its counterpart in the truncation of the periodic system, as shown in eq. (2.36). For $\lambda < 1$, we can employ a Bogoliubov transformation analogous to eq. (2.13):

$$u^2 = \frac{1}{2} \left(\frac{1 - \frac{\lambda}{2}}{\sqrt{1 - \lambda}} + 1 \right), \quad v^2 = \frac{1}{2} \left(\frac{1 - \frac{\lambda}{2}}{\sqrt{1 - \lambda}} - 1 \right). \quad (3.3)$$

We arrive at

$$\hat{H} = \sqrt{1 - \lambda} \hat{n}^b, \quad (3.4)$$

which coincides with the Bogoliubov Hamiltonian of either of the $|k| = 1$ -modes of the truncation of the periodic system to three modes (see eq. (2.37)). This represents a motivation for constructing our prototype model as shown in eq. (3.1).

For $\lambda < 1$, it follows from eq. (3.2) that depletion is given by

$$N_d = \frac{1}{2} \left(\frac{1 - \frac{\lambda}{2} \left(1 - \frac{N_d}{N}\right)}{\sqrt{1 - \lambda} \left(1 - \frac{N_d}{N}\right)} - 1 \right), \quad (3.5)$$

where as above we took into account backreaction. This coincides with the result (2.32) of the truncated periodic system, up to a factor of $1/2$, which accounts for the fact that the system (3.1) only has one non-zero mode instead of two. Therefore, depletion is still small and quantum breaking does not take place in the undercritical regime of the system (3.1).

In order to enhance depletion, we shall introduce Q species for the \hat{a}_1 -mode:¹¹

$$\boxed{\hat{H} = \sum_{k=1}^Q \left(\hat{n}_k - \frac{\alpha}{4} \left(2\hat{n}_0 \hat{n}_k + \hat{a}_0^{\dagger 2} \hat{a}_k^2 + \hat{a}_k^{\dagger 2} \hat{a}_0^2 \right) \right) + \frac{C_m}{2} \sum_{k=1}^Q \sum_{l=k+1}^Q f(k, l) \left(\hat{a}_k^{\dagger 2} \hat{a}_l^2 + \text{h.c.} \right)}. \quad (3.6)}$$

This Hamiltonian defines our new prototype model (NPM) that we shall study in the following. As is evident from eqs. (3.2) and (3.4), exclusively occupying the \hat{a}_0 -mode has the same effect in our new prototype model (3.6) as in the periodic system (2.9): For $\lambda < 1$, the corresponding state (2.10) coincides with the ground state in the mean-field limit where a classical instability appears for $\lambda > 1$.

¹¹This system is very similar to the full periodic model (2.9), if one replaces $k^2 \rightarrow 1$ in the kinetic terms. So one might also consider using such a periodic model with modified energy gaps.

A final remark is in order concerning the second line of eq. (3.6). In an analogous approach as in [64], we introduced this interaction to ensure that the system possesses no symmetries other than the conservation of total particle number. We choose the same $f(k, l)$ as in [64], which takes essentially random values in $|f(k, l)| \in [0.5; 1]$ with both positive and negative signs.¹² As we shall demonstrate subsequently, the value of C_m does not influence the system in any essential way, provided that C_m is not too large. We give some analytic estimates regarding this requirement in appendix A. In the numerical study, we shall moreover check empirically that the values of C_m that we consider do not change the qualitative behavior of the system.

3.2 Undercritical regime

As long as C_m is not too large, we can approximate the \hat{a}_k -modes, $k \geq 1$, as decoupled from each other. Then for each mode, the Bogoliubov approximation is still given by eq. (3.2) so that the number of depleted particles is enhanced by a factor of Q as compared to eq. (3.5):

$$N_d = \frac{Q}{2} \left(\frac{1 - \frac{\lambda}{2} \left(1 - \frac{N_d}{N}\right)}{\sqrt{1 - \lambda \left(1 - \frac{N_d}{N}\right)}} - 1 \right). \quad (3.7)$$

For $N_d \ll N$, the solution is

$$N_d = \frac{Q}{2} \left(\frac{1 - \frac{\lambda}{2}}{\sqrt{1 - \lambda}} - 1 \right) \left(1 - \frac{\lambda^2 Q}{8(1 - \lambda)^{3/2} N} + O\left(\frac{N_d^2}{N^2}\right) \right). \quad (3.8)$$

This clearly indicates that quantum breaking can take place for sufficiently large Q .¹³ For $\lambda \ll 1$, we can approximate

$$N_d \approx \frac{Q\lambda^2}{16}. \quad (3.9)$$

in accordance with eq. (2.18).

We proceed to make an estimate of the quantum break-time. As in the periodic system, we consider the process in which two particles of the \hat{a}_0 -mode annihilate to produce two excitations with $k \geq 1$. The introduction of Q channels in the final state enhances the rate (2.19) as

$$\Gamma = QN^2\alpha^2 = Q\lambda^2. \quad (3.10)$$

¹²Concretely, the function is [64]: $f(k, l) = \begin{cases} F(k, l) - 1 & \text{for } F < 0.5 \\ F(k, l) & \text{for } F \geq 0.5 \end{cases}$, where $F(k, l) = (\sqrt{2}(k-1)^3 + \sqrt{7}(l-1)^5) \bmod 1$. We remark, however, that the structure of the self-interaction of the \hat{a}_k -modes is different as compared to [64].

¹³Additionally, we can read off from eq. (3.8) an estimate for the coefficient of corrections that scale as $1/N$. We get $\lambda^2 Q / (8(1 - \lambda)^{3/2})$.

Consequently, the timescale after which a significant numbers of particles has left the \hat{a}_0 -mode is (see also [49, 146, 154] for the effect of species on the quantum break-time)

$$t_q = N\Gamma^{-1} = \frac{N}{Q\lambda^2}, \quad (3.11)$$

in accordance with eq. (2.21). At first sight, it appears that we have constructed a system that exhibits quantum breaking without any classical instability.

Comparing eqs. (3.9) and (3.11) reveals an immediate problem. Quantum breaking corresponding to a full deviation from the classical solution requires $N_d \sim N$, which leads to $Q \gtrsim N/\lambda^2$. Once Q is so large, however, eq. (3.11) implies $t_q \lesssim 1$. This means that the quantum break-time is shorter than the timescale of a single free oscillation. (We recall that our choice of units is such that $\hbar^2/(2mR^2) = 1$.) Therefore, one cannot say that a viable classical description existed to begin with and the meaning of quantum breaking becomes unclear. This issue is particularly evident in the classical limit $\hbar \rightarrow 0$. Generically, we know the scaling $N \sim \hbar^{-1}$ (see [45, 49]). Since full quantum breaking requires $Q \gtrsim N/\lambda^2$, it follows that $Q \sim N \sim \hbar^{-1}$. Then eq. (3.11) implies that $t_q \sim \hbar^0$, i.e., the quantum break-time would not vanish in the classical limit $\hbar \rightarrow 0$. Clearly, this does not make sense.

The above argument was first applied in quantum gravity [105–107]: Requiring that at least one emission of a Hawking quantum can be well-described semi-classically leads to an upper bound on the number of hidden species. Recently, this finding was connected to a breakdown of perturbative unitarity [155–157] (see [158, 159] for concrete models). Namely, taking into account Q species effectively enhances coupling constants by powers of Q . Therefore, perturbation theory only remains valid if Q is not too large.¹⁴

For our present discussion, the availability of a perturbative approximation is not essentially since we shall study our system by exact non-perturbative means. As discussed above, however, $t_q \ll 1$ would put into question the meaning of quantum breaking. Still, there are several caveats in the above argument. First, it is unclear if in all parts of parameter space the number N_d of depleted particles can give reliable information about dynamical properties and time evolution. Second, formula (3.9) is no longer valid close to $\lambda = 1$. Therefore, it is conceivable that undercritical quantum breaking can take place if λ is sufficiently close to 1. Third, findings for $Q \gg N$ have meaning for systems with finite parameters and finite \hbar , independently of their limiting behavior. While these questions remain to be answered, it is important to emphasize that our NPM is a consistent quantum system for all values of Q and our numerical analysis of time evolution is viable for all parameter choices.

3.3 Overcritical regime

Next, we shall consider the overcritical regime $\lambda > 1$. As is evident from eq. (2.30), the number of depleted particles scales with N already for $Q = 1$. Therefore, the inclusion of

¹⁴Applied to our system, it appears that including Q species has the same effect as replacing the coupling $\alpha \rightarrow \alpha_{\text{eff}} = \alpha\sqrt{Q}$ (see e.g., the process shown in fig. 2). Then $Q \sim N/\lambda^2$ leads to $\alpha_{\text{eff}} = 1/\sqrt{N}$, which still allows for a perturbative expansion.

additional species does not change this finding. In order to obtain an estimate for the quantum break-time, we take into account the effect of species in the rate (2.26):

$$\Gamma = Q\lambda^2 + Q\sqrt{\lambda-1}\Delta N. \quad (3.12)$$

As in eq. (3.10), the initial rate is enhanced by a factor of Q . In order to decide which of the two terms dominates, we shall study what maximal value of ΔN could be obtained. If the second term in eq. (3.12) dominates, then ΔN is determined by the point when the instability disappears due to backreaction. As derived in eq. (2.31), this leads to

$$\Delta N_{\text{inst.}} = N(\lambda - 1)/\lambda. \quad (3.13)$$

Crucially, $\Delta N_{\text{inst.}}$ is independent of Q . Therefore, one can expect that for sufficiently large Q , the first term in (3.12), corresponding to perturbative scatterings, becomes important. In this parameter regime, we use eq. (3.7) to obtain the estimate¹⁵

$$\Delta N_{\text{pert.}} \approx \frac{\sqrt{QN\lambda}}{4}. \quad (3.15)$$

Accordingly, we can try to estimate the quantum break-time. If the instability dominates, the enhancement of the rate by Q in eq. (3.12) leads to an additional factor of $1/Q$ in t_q as compared to (2.28). The situation is more involved for sufficiently large Q . One could try to employ the result (3.11) of the undercritical regime but this would amount to completely neglecting the instability and the second term in eq. (3.12). Clearly, this cannot be the case, which prevents us from making an analytic statement for large Q . In total, depending on whether (3.13) or (3.15) dominates, we estimate the quantum break-time as

$$t_q = \begin{cases} \frac{\ln N}{Q\sqrt{\lambda-1}} & Q \ll 16N \frac{(\lambda-1)^2}{\lambda^3} \\ \text{???} & Q \gg 16N \frac{(\lambda-1)^2}{\lambda^3} \end{cases}, \quad (3.16)$$

where only the numerical study will allow us to derive a conclusion about the regime of large Q . Moreover, we note that the interpretation of the regime $Q \gg N$ may cause problems. In analogy to our discussion of undercritical quantum breaking, it is possible that this parameter space leads to a quantum break-time that does not become infinite in the classical limit $\hbar \rightarrow 0$. Finally, we must emphasize that all the above formulas only represent heuristic estimates. Whether or not they are valid will be determined by our subsequent numerical investigation.

¹⁵First, we assume $N_d \ll Q \ll \lambda N$ to derive from eq. (3.7):

$$\left(1 - \lambda \left(1 - \frac{N_d}{N}\right)\right) N_d = \frac{Q\lambda^2}{16}. \quad (3.14)$$

We can solve this quadratic equation and obtain eq. (3.15) for sufficiently small $\lambda - 1$.

3.4 Critical regime

In the critical case $\lambda = 1$, we will again use an extrapolation of the undercritical formula (3.7) to estimate the number of depleted particles. This yields

$$N_d = \frac{Q^{2/3}N^{1/3}}{2^{4/3}} \left(1 + O\left(\frac{1}{N^{2/9}}\right) \right), \quad (3.17)$$

i.e., including Q overcritical species enhances depletion by a factor of $Q^{2/3}$ (cf. eq. (2.33)). We expect that the dependence $t_q \sim \sqrt{N}$ of the quantum break-time shown in eq. (2.34) persists but we are unable to provide an analytic estimate regarding the influence of Q on this scaling.

4 Numerical study

Now we turn to the numerical study of the prototype model (3.6). To this end, we employ the software *TimeEvolver* [108], which is capable of computing real-time evolution with adjustable error bound for generic quantum system of Hilbert space dimension up to $\sim 10^7$. Generically, we set in the following the bound on $\|v_{\text{num}}(t) - v(t)\|$ to be 10^{-6} , where $v_{\text{num}}(t)$ is the output of *TimeEvolver* and $v(t)$ corresponds to the exact state at time t . For selected parameters, corresponding to very large Hilbert spaces, we use as tolerance 10^{-4} , mainly due to an effect of finite machine precision. We plot data obeying the stricter error bound with black dots while results obtained with a 10^{-4} tolerance are depicted in gray. Unless stated otherwise, we compute the expectation value of observables in intervals of $t_{\text{step}} = 0.01$. All numerical data presented subsequently are publicly available in the companion Zenodo record [160]. The code to generate the data is available in the complementary github repository [161].

The feasibility of numerical simulation is mainly limited by Hilbert space dimension. In order to reduce the size of the problem, we introduce a maximal occupation C for the \hat{a}_k -modes, $k \neq 0$. This is also empirically motivated since in some situations these modes are not highly occupied. However, we set value of C so high that it does not qualitatively influence the behavior of the system. We can ensure that this property is fulfilled by increasing C until its effect becomes negligible.

In the following analysis we will denote the expectation value of an operator \hat{n}_k with the same symbol but without the hat: $\langle \hat{n}_k \rangle = n_k$. As initial state, we employ (2.10), corresponding to all particles in the \hat{a}_0 -mode, $\langle \text{in} | \hat{n}_0 | \text{in} \rangle = N$. As discussed above, the advantage of using this state is that evaluating the expectation value $\langle \hat{n}_0 \rangle$ is sufficient for determining departure from the classical solution. Quantum breaking occurs as soon as $\langle \hat{n}_0 \rangle$ deviates significantly from N .

4.1 Comparison of prototype model and periodic system

A motivation for constructing our NPM (3.6) consists in its similarity to the PPM of [32] in its truncated version (2.35). In particular, we have shown that the results of Bogoliubov

approximation coincide, cf. eqs. (2.36) and (3.2). We extend this comparison here to the full quantum Hamiltonians (2.35) and (3.6) for finite total occupation number N . Obviously, those two systems are not identical and so we do not expect indistinguishable result. We shall see, however, that dynamics are qualitatively very similar.

To verify this claim and quantify the difference for finite N , we perform numerical simulations for both the under- and overcritical regime corresponding to the collective coupling values $\lambda_u = 0.8$ and $\lambda_o = 1.2$, respectively. Moreover, we set the total particle number in both systems to be $N = 10$. Since the truncated PPM (2.35) features two modes with non-zero momentum, we set $Q = 2$ in the NPM. In both models we set the capacity C equal to the number of particles to exclude any influence originating from finite maximum occupation numbers. We also set the symmetry-breaking coupling in the NPM to zero, $C_m = 0$ to keep the symmetry between the \hat{a}_1 and \hat{a}_2 mode in analogy to the momentum conservation constraint in the PPM that forces $n_{-1}(t) = n_1(t)$. We note, however, that the analogy between the NPM and the PPM is not complete. While the PPM features terms coupling the non-zero modes, those are completely absent in the NPM when we set $C_m = 0$. Our parameter choices are summarized in eq. (4.1) for the PPM and in eq. (4.2) for NPM:

$$\text{PPM (eq. (2.35))}: \quad \lambda = \{0.8, 1.2\}, \quad N = 10, \quad C = 10, \quad (4.1)$$

$$\begin{aligned} \text{NPM (eq. (3.6))}: \quad \lambda = \{0.8, 1.2\}, \quad N = 10, \quad C = 10, \quad (4.2) \\ Q = 2, \quad C_m = 0. \end{aligned}$$

The realtime evolution of the occupation numbers of the \hat{n}_0 - and \hat{n}_1 - operators for both systems are plotted in fig. 3. Note that due to a shift symmetry and corresponding momentum conservation $n_1 = n_{-1}$ in the PPM. In contrast, n_2 in the NPM is generically only restricted by particle number conservation, such that $n_2 = N - n_0 - n_1$. We observe that in both cases the systems exhibits very similar qualitative and quantitative behavior. In particular, frequency and amplitude are of the same order of magnitude.

4.2 Undercritical regime

Having shown that the truncated PPM (2.35) and the NPM (3.6) exhibit very similar dynamics, we shall only consider the latter in the following. As discussed in sections 2 and 3, this model does not exhibit quantum breaking in the undercritical regime without additional species, i.e., for $Q = 1$. This is because the system both only shows very small deviations from the initial state as well a strong tendency to return to it on the natural frequency of the system. We argued, however, in section 3 that the introduction of additional species or decay channels can result in a strong deviation from the initial state without recurrence.

In order to show that this is indeed the case, we perform numerical simulations for various values of Q . For breaking the symmetry between different modes, we also turn on the

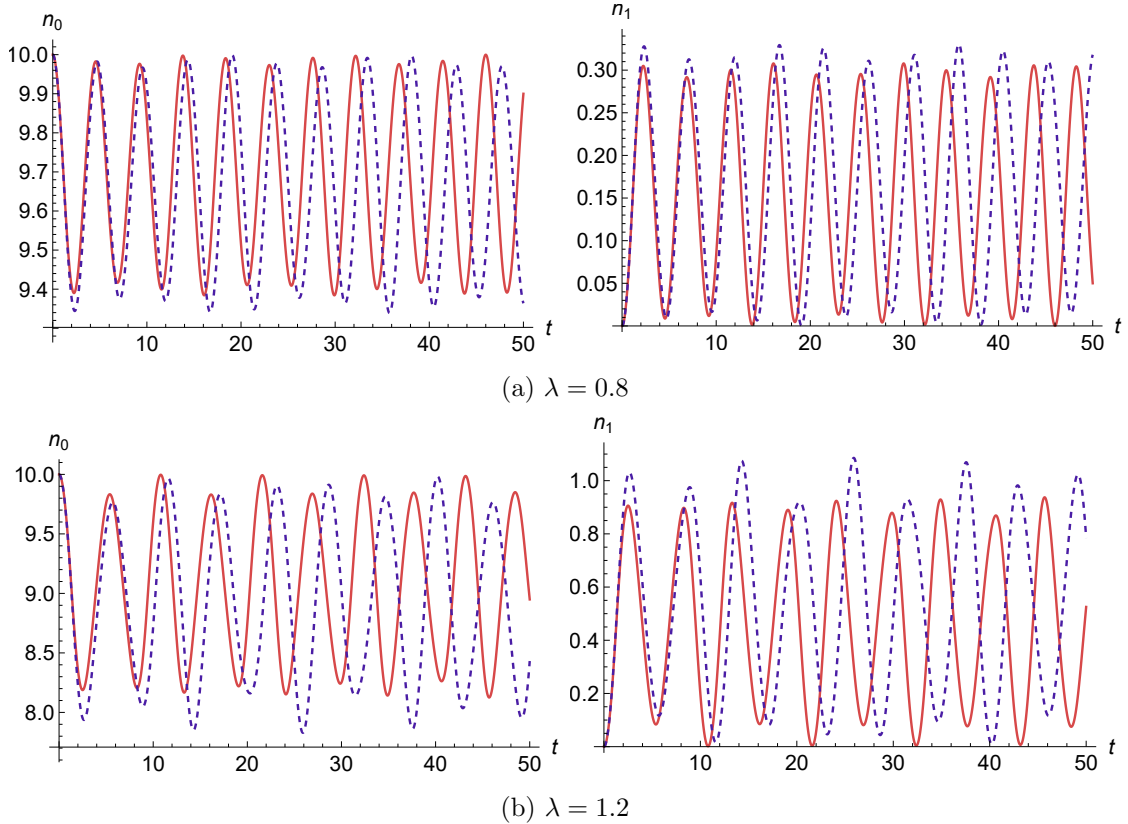


Figure 3: Time evolution of expectation values of the particle number operator n_0 (left side) and n_1 (right side) with initial state (2.10) and parameter values set by (4.1) and (4.2). The upper row depicts the undercritical regime $\lambda_u = 0.8$ while the lower row shows the evolution in the overcritical regime $\lambda_o = 1.2$. The PPM (2.35) is depicted with a dashed blue line while the NPM (3.6) is drawn in red. Both systems show similar dynamics in terms of frequency and amplitude.

inter-species coupling C_m . The specific choices of parameters are given by

$$\lambda = 0.8, \quad N = 10, \quad C_m = 0.1, \quad C = 4. \quad (4.3)$$

We set $C < N$ this time but in the undercritical regime modes different than n_0 only get very sparsely occupied so that we do not expect the truncation of maximal occupation to have a significant impact. We will confirm this later in various other scans. For different values of Q , we display the expectation value of the \hat{n}_0 as a function of time in fig. 4. We observe that for $Q = 1$, no quantum breaking takes places (see fig. 4a), i.e., $\langle \hat{n}_0 \rangle$ always stays close to its initial value and returns to it on its free frequency timescale. However, this changes distinctly for sufficiently large Q . We observe that the expectation value of \hat{n}_0 deviates significantly from

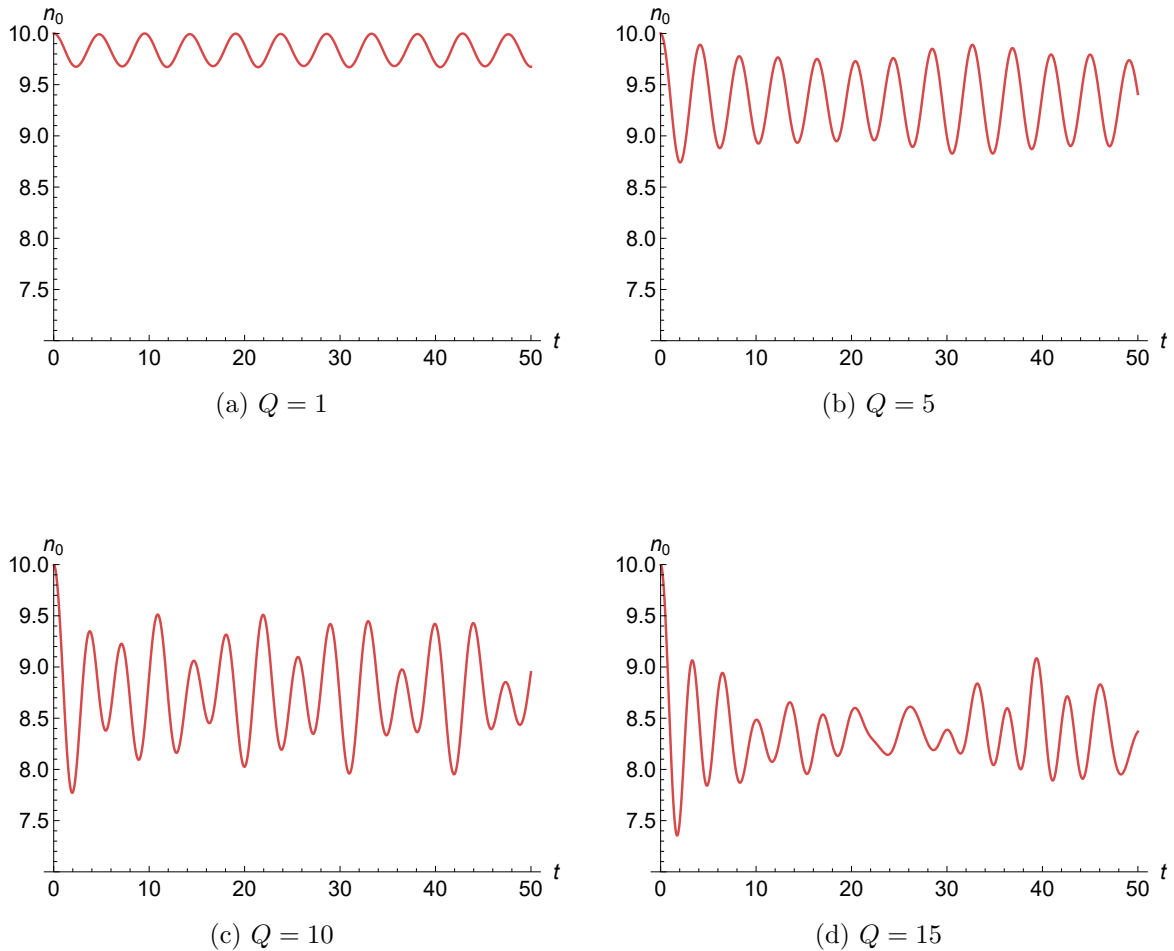


Figure 4: Time evolution of the initial state (2.10) for different values of Q . All other parameters are set by eq. (4.3). The plots show the expectation value of \hat{n}_0 as function of time. While $Q = 1$ leads to recurrence to the initial configuration, the phenomenon disappears for larger values of Q .

its initial value as soon as $Q \gtrsim 10$ (see fig. 4c). Moreover, it never returns to the initial state. Thus, the explicit numerical study confirms that the NPM (3.6) exhibits quantum breaking without the presence of a classical instability.

After we confirmed that introducing an sufficient amount of additional modes can lead to quantum breaking, we shall next investigate quantitatively how the timescale of quantum breaking depends on the different parameters of the system. Most important will be the dependence on the total particle number N . Since the consideration in section 3 are only valid for large N , we shall choose bigger values of N as compared to eq. (4.3). Correspondingly, C_m needs to be sufficiently small in order not to change the qualitative behavior of the system (see appendix A). These considerations can be taken into account with the following choice

of parameters

$$\lambda = 0.8, \quad N = 50, \quad C_m = 0.016, \quad C = 4, \quad Q = 10. \quad (4.4)$$

For the subsequent analysis, we define quantum breaking as follows: Over the range of parameters $X \in \{Q, N, \alpha, C_m\}$ that we consider, we simulate the dynamics of the system (3.6) with the initial state given by eq. (2.10) until $t_{\max} = 50$. We determine in each case the minimal relative occupation of the \hat{n}_0 mode,

$$r_{\min}(X) = \min_t \frac{\langle \hat{n}_0(t) \rangle}{N}, \quad (4.5)$$

where the dynamics and therefore the minimal occupation value depends on the parameters X of the system considered. To define a common threshold deviation from the initial occupation number of \hat{a}_0 , we require it to be crossed for all values of X in question. Correspondingly, we define quantum breaking as the timescale t_q after which the relative occupation of the zero mode, n_0/N , falls for the first time below

$$b_{th} = 1 - (1 - \max_X n_{\min}(X)) \cdot 0.8. \quad (4.6)$$

Since not only the timescale but also the maximal amplitude will generally depend on the precise value of all parameters, this definition can only be meaningful over a finite interval. If this interval is chosen too wide, comparing the timescale for crossing a fixed threshold can become meaningless: A value of b_{th} that is close to the maximal amplitude in one case may correspond to only a small deviation from the initial state for a different choice of parameters. Therefore, the threshold should be chosen such that it is not much smaller than the minimal value of n_0/N for all values of the parameter in the interval considered. In order to ensure that this condition is fulfilled, we present next to each scan also the a plot of the maximum relative depletion until t_{\max} and the corresponding threshold.

Dependence on N First, we investigate the scaling of the break-time with the total particle number N . To this end, we perform numerical simulations for the undercritical regime with parameter choices (4.4) while varying the conserved particle number N . As shown in eq. (3.11), analytic arguments suggest a linear scaling. This is confirmed in our simulation, as is evident from fig. 5, where we scan over $50 \leq N \leq 250$ and following that perform a linear fit of the form

$$t_q = m \cdot x + n, \quad (4.7)$$

with fit parameters m , n and $x = N$. Fitting the data yields the following values

$$m = 0.0059, \quad n = 0.51. \quad (4.8)$$

We also fit a polynomial function of the form

$$t_q = a \cdot x^c + b, \quad (4.9)$$

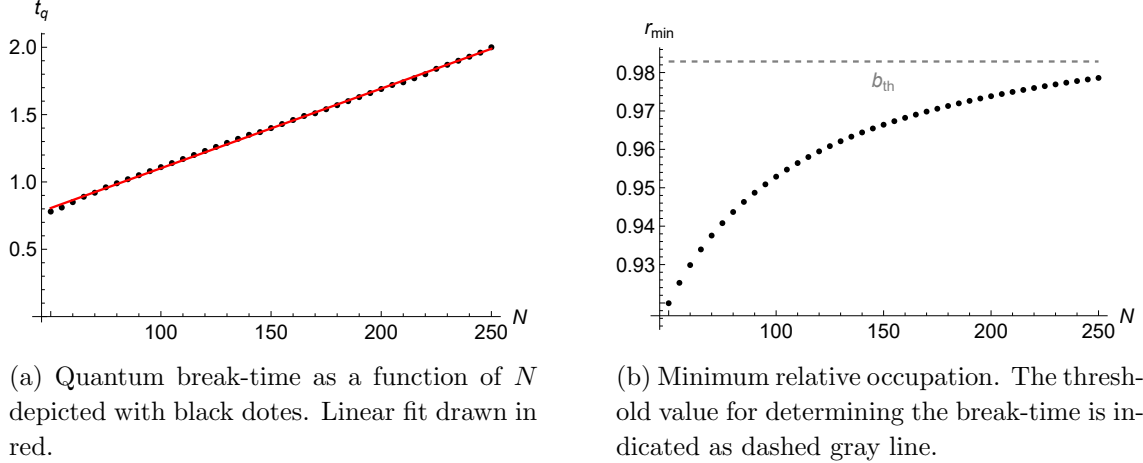


Figure 5: N -Scan in the undercritical regime for $\lambda = 0.8$ with remaining parameters values set by eq. (4.4). The quantum break-time as a function of N is shown on the left side and the corresponding threshold values for the amplitude are on the right side. We observe a linear dependence between the total particle number N and the quantum break time t_q .

with fit parameters a, b, c in order to quantify the deviation from linearity. Fitting the data with a function of the form (4.9) yields

$$a = 0.0095, \quad b = 0.44, \quad c = 0.92. \quad (4.10)$$

The exponent c close to 1 indicates a linear relation between the particle number N and the break-time t_q .

As discussed above, we are required due to numerical limitation to limit the maximal occupation of every mode. To check that we choose this capacity large enough to not have a qualitative effect on our findings, we repeated this analysis for higher $C = 6$ in the appendix B (see fig. 12c). Moreover, we performed simulations for small $10 \leq N \leq 50$ in fig. 12a and large $1000 \leq N \leq 5000$ in fig. 12b as well as $C_m = 0$ in fig. 12d. We observe that the linear behavior is maintained in all these examples. In particular, it does not depend qualitatively on a specific N range or the inter-species coupling C_m . More details are shown in appendix B.

Dependence on Q Next, we investigate the scaling with the number of species Q . With the same parameter choice (4.4), we perform a scan for $Q \in \{15, 16, \dots, 29, 30\}$ and fit a polynomial function of the form eq. (4.9), where now $x = Q$. In agreement with eq. (3.11), we observe (within numerical uncertainties) the following scaling

$$t_q \sim Q^{-1.0}. \quad (4.11)$$

The data as well as the fit details can be found in the appendix B. Moreover, we perform a second Q -scan with lower particle number $N = 10$ (and adjusted inter-species coupling C_m),

which yields similar numerical values indicating the robustness of our results. We remark, however, that including smaller Q in the fit increases the exponent. This can partly be attributed to threshold ambiguities but even besides that the fitting is not fully stable. The figures for both fits can be found in the appendix, see figs. 13a and 13b, respectively.

Dependence on λ Inspecting eq. (3.11) suggests an quadratic reciprocal scaling of the break-time with respect to the collective coupling λ . As explained at the beginning of this section, fitting over intervals in which the amplitude of n_0 changes significantly is not meaningful since no common threshold for defining quantum breaking can be found. Therefore, we split the fit in two intervals and fit over the regimes $0.2 \leq \lambda \leq 0.5$ and $0.5 \leq \lambda \leq 0.9$ separately. We obtain following values

$$t_q \sim \begin{cases} \lambda^{-1.8} & 0.2 \leq \lambda \leq 0.5, \\ \lambda^{-2.2} & 0.5 \leq \lambda \leq 0.9, \end{cases} \quad (4.12)$$

which both lie near the analytically expected value of $c = -2$. Details and the corresponding figs. 14a and 14b can be found again in the appendix. We remark that we increase the sampling step to $t_{\text{step}} = 0.001$ for this scan as well as for the subsequent investigation of the dependence on C_m .

Dependence on C_m As remaining parameter we investigate the dependence on the inter-species coupling C_m . This parameter is not present in the PPM discussed in section 2, where the interaction strength between different momentum modes is determined by the overall coupling constant α . We usually set C_m large enough to break the symmetry between the different species appreciably but at the same time small enough not to have a large influence on the dynamics. As is evident from fig. 14c in the appendix, our parameter choice fulfills this condition and the break-time exhibits only marginal sensitivity towards C_m .

4.3 Overcritical regime with few species

After analyzing the undercritical regime we next investigate the overcritical phase with $\lambda > 1$. As discussed in section 3.3, we expect that the overcritical phase can be divided in two distinct regimes depending on the number of modes Q in comparison with the total particle number N and collective coupling λ . In this section we will first explore the case when there are only few species available to offload occupation numbers with respect to the total number of transferred particles, corresponding to the first line in eq. (3.16).

It is known that due to the development of an instability the overcritical regime exhibits quantum breaking even without the introduction of additional species [10]. Nevertheless, we first want to give a qualitative picture of how the dynamic is influenced by the introduction of more decay channels. To this end, we again show the realtime evolution of the expectation value of the number operator \hat{n}_0 for different values of Q . The parameters are set by

$$\lambda = 1.2, \quad N = 50, \quad C_m = 0.016, \quad C = 50, \quad Q = 3. \quad (4.13)$$

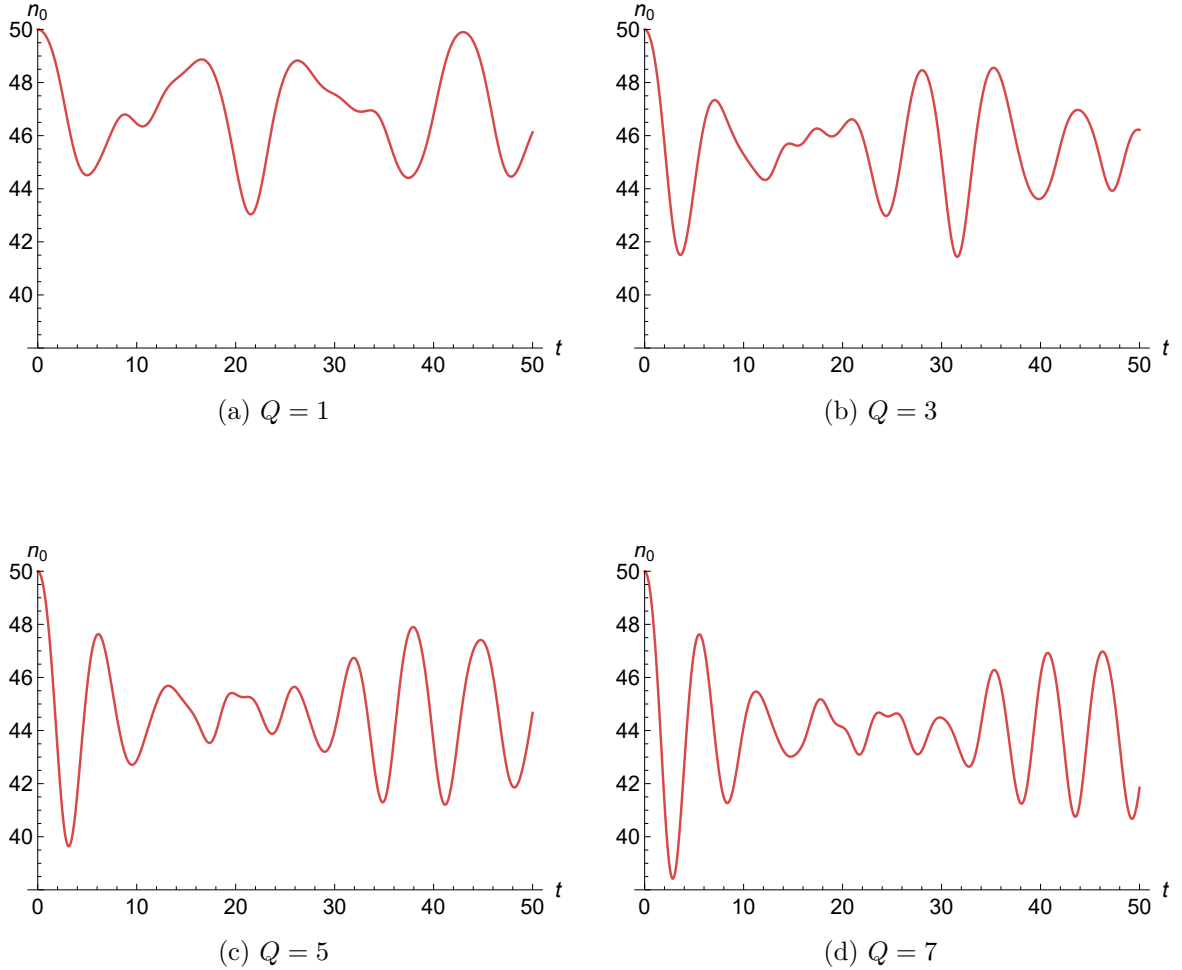
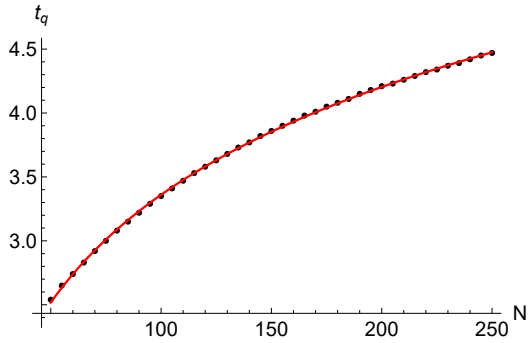
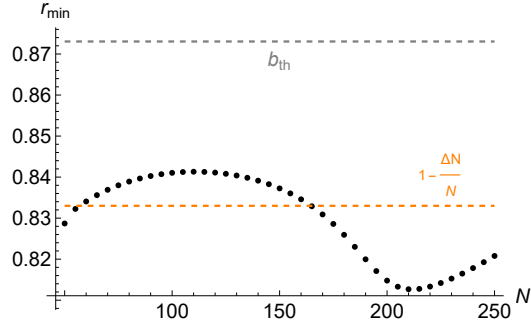


Figure 6: Time evolution of the initial state (2.10) for different values of Q in the overcritical regime $\lambda = 1.2$ for small Q . All other parameters are set by eq. (4.13). The plots show the expectation value of \hat{n}_0 as function of time. While $Q = 1$ already leads to quantum breaking, increasing Q enhances this effect.

This choice fulfills the heuristic criterion shown in eq. (3.16), i.e., $Q \ll 16N(\lambda - 1)^2/\lambda^3$. Since depletion is much stronger in the overcritical regime, we do not limit the occupation of the modes with $k \geq 1$ in order not to spoil our findings by finite capacity effects. The results of time evolution for different values of Q are displayed in fig. 6. We observe that the system exhibits quantum breaking already for $Q = 1$ in contrast to the undercritical regime, where breaking could only be realized by the introduction of a sufficient number of species. This is in line with previous results on the PPM, in which breaking was only observed in the overcritical regime [10, 48]. However, although quantum breaking is already possible in the absence of additional species for $\lambda > 1$, introducing more channels still increases the amplitude and shortens the timescale.



(a) Quantum break-time as a function of N depicted with black dots. Logarithmic fit drawn in red.



(b) Minimum relative occupation. The threshold value for determining the break-time is indicated as dashed gray line. Turning point due to backreaction to the collective coupling in orange (see eq. (2.31)).

Figure 7: N -Scan in the overcritical regime for $\lambda = 1.2$ with remaining parameters values set by eq. (4.13). Quantum break-time as a function of N on the left side and the corresponding threshold values for the amplitude on the right side. We observe a logarithmic dependence between the total particle number N and the quantum break time t_q .

Next, we investigate the system quantitatively and scan again over the different parameters, where in each case the remaining parameters are set by eq. (4.13). In addition to a polynomial fit function (4.9), we will also use a logarithm function of the form

$$t_q = p \cdot \log(x) + q, \quad (4.14)$$

with fit parameters q and p .

Dependence on N First we study again the dependence of the break-time on the total particle number N . We show the data and fit for the value range $50 \leq N \leq 250$ in fig. 7. In agreement with eq. (3.16), we observe a logarithmic scaling with the fit parameters

$$p = 1.22, \quad q = -2.24. \quad (4.15)$$

Again we perform additional scans to check the generality of our findings. First we increase the numerical parameter C to verify that we set the capacity high enough to not spoil our findings. Moreover, we also check that the interspecies coupling has no significant quantitative influence by repeating the analysis with $C_m = 0$. Both checks yields almost identical results. The difference to the fit depicted in fig. 7 is minuscule. The data, fits and plots can again be found in appendix C, see fig. 15b for $C = 60$ and see fig. 15a for $C_m = 0$.

Dependence on Q After finding the previously known scaling with $\ln N$, we now turn to the other parameters. We start again with the dependence on the number of species Q . We use eq. (4.13) as base values and perform a scan over increasing Q . Unfortunately, due

to the exponential scaling of the Hilbert space with Q and the corresponding increase in demand of computational resources, we are very limited in the size of Q we can simulate. Correspondingly, we perform a scan over $2 \leq Q \leq 8$.¹⁶ The result is plotted in fig. 16a and can be found with the corresponding details in the appendix. Selected realtime plots have already been shown in the beginning of this section in fig. 6. In summary we find the following dependence

$$t_q \sim Q^{-0.84}, \quad (4.16)$$

which is close to the expected value $c = -1$ of eq. (3.16). We want to stress, however, that the fit is not fully stable and the exponent of Q can vary depending on the fit range.

Dependence on λ Next, we scan over the collective coupling λ , where we limit ourselves to the interval $1.2 \leq \lambda \leq 1.6$. In this regime, we expect the scaling $\frac{1}{\sqrt{\lambda-1}}$ as shown in eq. (3.16). We therefore perform a fit of the form

$$a \cdot (x - d)^c, \quad (4.17)$$

which yields

$$t_q \sim \frac{1}{(\lambda - 0.88)^{0.49}}, \quad (4.18)$$

in very good agreement with the analytic expectations. For details and figures we refer the reader to fig. 16b in the appendix.

Dependence on C_m In analogy to the undercritical case, we want to verify that C_m does not play a significant role in the dynamics, as long as the bounds of appendix A are maintained. For this purpose, we scan over $0.01 \leq C_m \leq 0.09$. In this interval, the change of the break-time is only of order $\sim 10^{-3}$, as is evident from fig. 16c in the appendix.

4.4 Overcritical regime with many species

Finally, we want to study the overcritical regime with a large number Q of modes. We implement this by the following numerical choice of parameters

$$\lambda = 1.2, \quad N = 10, \quad C_m = 0.08, \quad C = 16, \quad Q = 10, \quad (4.19)$$

which fulfill the heuristic criterion shown in eq. (3.16), i.e., $Q \gg 16N(\lambda - 1)^2/\lambda^3$. Moreover, we note that we set $C > N$ in order to accommodate for higher N in the N -scan. Due to computational limitations, large Q requires us to use this relatively small C which can have a quantitative influence on the time evolution of the system. However, we will again verify that the results are still qualitatively independent of the specific choice of C . Exploring the second overcritical regime is especially computationally intensive since the Hilbert space dimension scales exponentially with Q and Q needs to be sufficiently large as compared to N over the

¹⁶Note that we excluded $Q = 1$ since in this case a larger amplitude of n_0 was reached after the system recurred closely to the initial state.

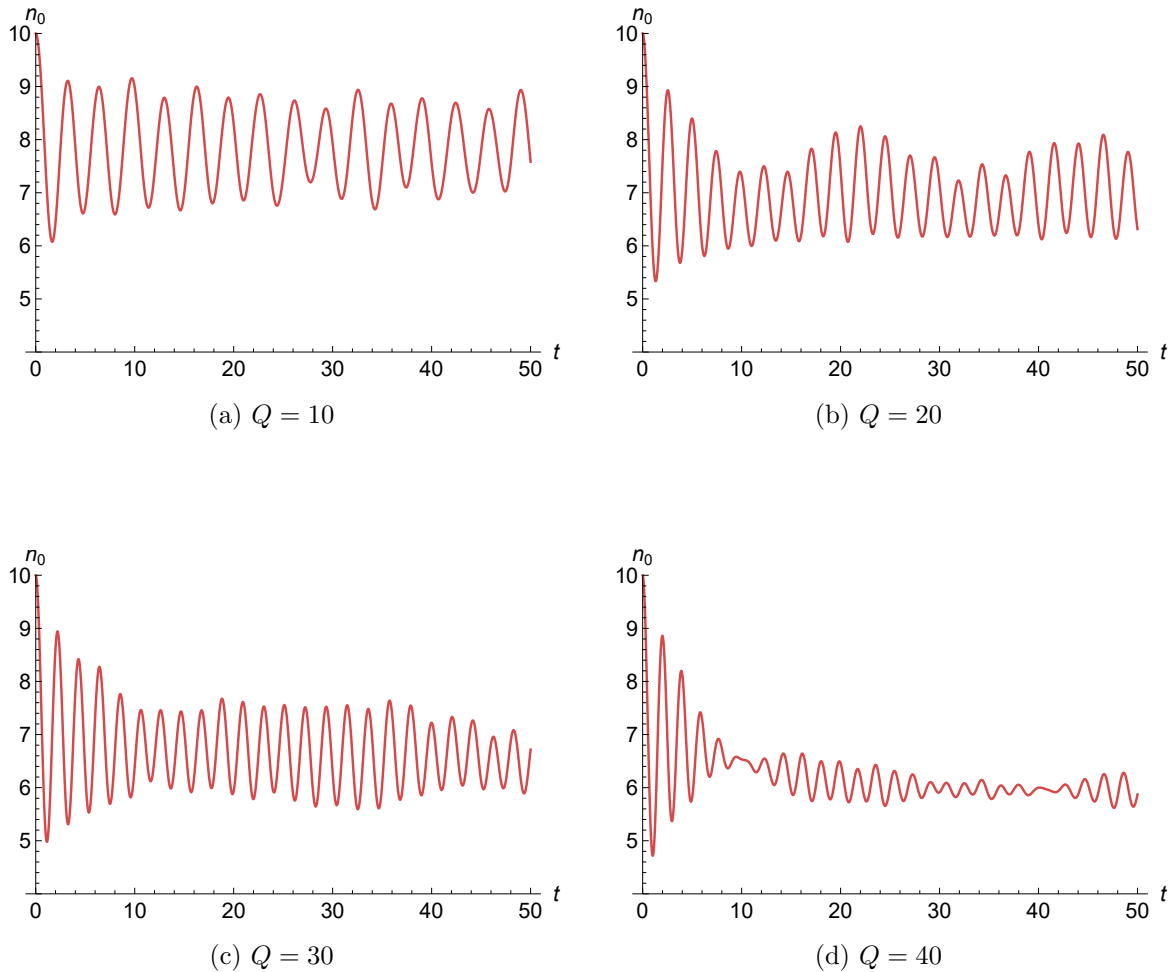


Figure 8: Time evolution of the initial state (2.10) for different values of Q in the overcritical regime $\lambda = 1.2$ for large Q . All other parameters are set by eq. (4.19). The plots show the expectation value of \hat{n}_0 as function of time. Increasing Q enhances the breaking effect.

whole scan range. On the other hand, N cannot be too small to avoid finite size effects scaling as $1/N$.

We start again by showing selected real time plots for various numbers of species Q in fig. 8. Since we start in the overcritical regime (and have large Q) all plots exhibit quantum breaking. Similar to the case of few Q discussed in the last section, increasing the number of channels enhances the breaking effect significantly. This effect is particularly strong in fig. 8d.

Dependence on N We start again with the dependence on N . As discussed in section 3.3, we do not have a clear analytical expectations for this regime. We consider the parameter range $5 \leq N \leq 25$ and show the corresponding data in fig. 9. Performing again a polynomial

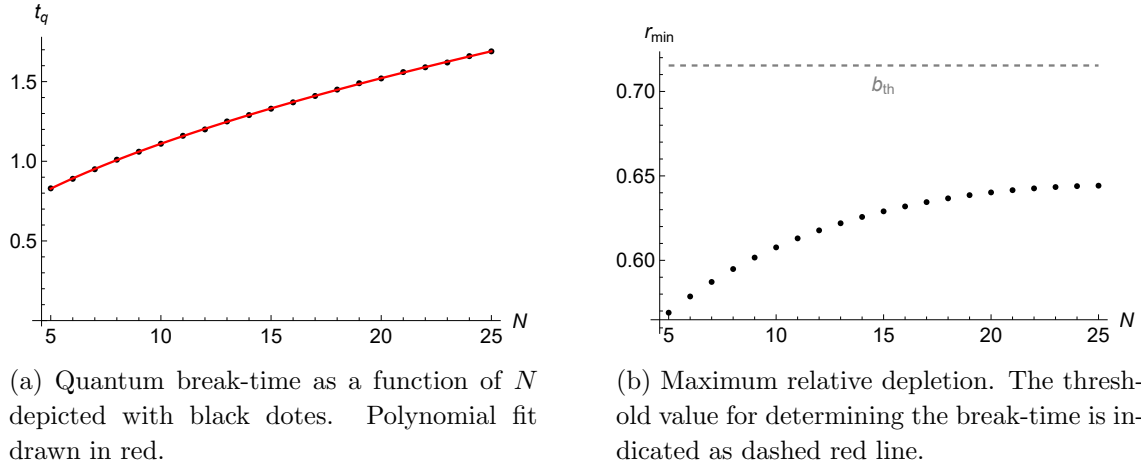


Figure 9: N -Scan in the overcritical regime for $\lambda = 1.2$ and many species with remaining parameters values set by eq. (4.19). Quantum break-time as a function of N on the left side and the corresponding threshold values for the amplitude on the right side. We observe that the quantum break-time t_q scales with the square root of the total particle number N .

fit, we find following values

$$a = 0.26, \quad b = 0.21, \quad c = 0.54. \quad (4.20)$$

Therefore, we get

$$t_q \sim N^{0.54}. \quad (4.21)$$

The numerical results suggest a dependence on the square root of the particle number (cf. eq. (1.5)). This is a novel regime distinct from the linear scaling in the undercritical phase and the logarithmic dependency in the overcritical phase with few species. However, we have to stress that the true value for the exponent might differ significantly from eq. (4.21). On the one hand, we both expect finite size effect due to a relatively low particle number N . On the other hand, the heuristic conditions for being in the regime of large species (see eq. (3.16)) is only marginally fulfilled close to $N \approx 25$ when $Q = 10$. Again we perform two additional consistency checks by performing N -scans for $C_m = 0$ and higher capacity $C = 20$. These can be found in the appendix D. The numerical values for the exponent in those scans are close to eq. (4.21), yielding further indications for the scaling $t_q \sim \sqrt{N}$.

Dependence on Q Next, we perform a scan over $15 \leq Q \leq 40$. More details can again be found in the appendix and the result is displayed in fig. 18a. Fitting the polynomial function (4.9), we observe the dependence

$$t_q \sim Q^{-0.67}. \quad (4.22)$$

This finding could indicate a scaling with $Q^{-2/3}$, which, however, remains to be verified.

Dependence on λ To determine the λ dependence, we compute the time evolution for several values in the interval $\lambda \in [1.1, 1.3]$. Again, we do not have a clear expectation and so we perform a shifted polynomial fit of the form eq. (4.17). This yields

$$t_q \sim \frac{1}{(\lambda - 0.66)^{0.6}}, \quad (4.23)$$

However, it is also possible to fit the data with a polynomial function of the form eq. (4.9). In this case the break-time scales as

$$t_q \sim \lambda^{-2.59}. \quad (4.24)$$

We observe behavior similar to the undercritical case (see eq. (4.12)) continuing the tendency of ever more negative exponent for larger λ . At the same time the data also indicate a divergent property at a critical point similar to the overcritical case with only few available species (see eq. (4.18)). At this point, we cannot conclusively determine the true scaling behavior of the collective coupling. Both eq. (4.23) and eq. (4.24) describe the data equally well. Details concerning the fits and the resulting figures can be found in the appendix (see fig. 19).

Dependence on C_m The final scan we perform is again over the interspecies coupling C_m . This time we vary its value such that $0 \leq C_m \leq 0.5$. Although the interval is relatively large, we observe again only marginal influence on the break-time t_q . The resulting fig. 18c can be found in the appendix.

4.5 Critical interpolation

So far, we have investigated the dependence of the quantum break-time on the total particle N for different regimes. We found a linear dependence in the undercritical regime $\lambda < 1$ and a logarithmic scaling for the overcritical case $\lambda > 1$ corresponding to a classical instability. In this final section, we study the transition between these two regimes. We will do this by performing several N -scans for different values of the collective coupling in the interval $0.8 \leq \lambda \leq 1.2$. The threshold amplitude is determined for each λ individually. We then perform fits to determine the interpolation between the previously observed linear and logarithmic scalings.

First, we have to find a set of values for the parameters that are physically meaningful throughout the phase transition and obey numerical limitations. Specifically, the implementation of quantum breaking in the undercritical regime requires the introduction of a sufficient number of additional species Q . Moreover, we also require N to be sufficiently large in order to avoid finite size effects. However, the overcritical regime also needs a large capacity $C \sim N$ in order not to spoil the logarithmic scaling. Ideally one would like to choose all these parameters sufficiently high, however, the exponential scaling of Hilbert space dimension makes this unfeasible. Therefore, we have to take a compromise here and we will vary the particle number within $50 \leq N \leq 150$ with the other parameters set by

$$C_m = 0.01, \quad C = 44, \quad Q = 5. \quad (4.25)$$

Note that $C = 44$ is already so small that it starts to influence dynamics close to $N = 150$ in the overcritical regime. Therefore, quantitative results should be interpreted with care. However, the qualitative transition from the undercritical to the overcritical regime can still be captured. In order to visualize the transition, we plot the break-time and fit a linear function in fig. 10a as well as a logarithm in fig. 10b. We conclude that while a linear fit describes the data very precisely for small $\lambda \lesssim 0.9$, it becomes increasingly less accurate for higher λ and does not provide a meaningful description for $\lambda \gtrsim 1.1$. Conversely, a logarithmic fit does not capture the break-time dependence on N in the undercritical phase but becomes increasingly precise in the overcritical regime.

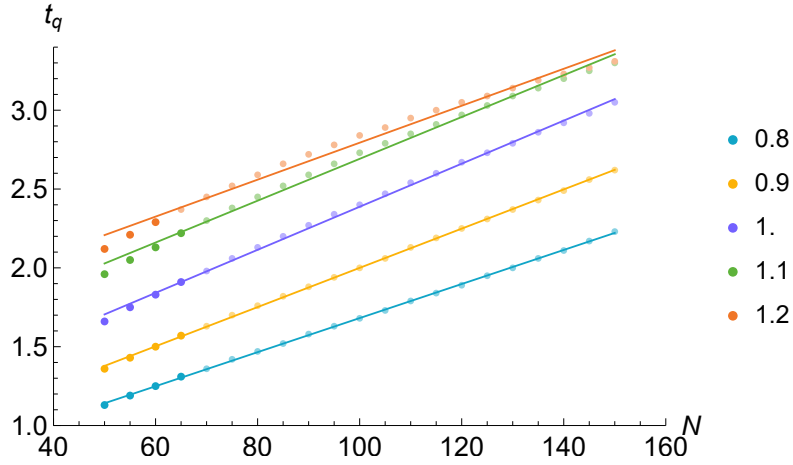
In addition to the qualitative behavior shown in fig. 10, we provide also a quantitative analysis of the transition between both phases. On top of a linear and log fit shown in figs. 10a and 10b, respectively, we also perform a polynomial fit of the form eq. (4.9) for each λ and plot the resulting exponent c in fig. 11. For $\lambda = 0.8$, the numerical value of the exponent is close to $c = 1$, in accordance with a linear scaling. In contrast, c is much smaller for $\lambda = 1.2$, which indicates a logarithmic dependence.¹⁷ When increasing λ from 0.8 to 1.2, the observed value of c decreases monotonously. This leads to a smooth interpolation between the linear and logarithmic scalings.

We want to note again that the threshold in fig. 10 was set for each λ individually. Since the threshold b_{th} as defined in eq. (4.6) deviates more significantly from 1 for higher λ , the break-time appears to increase. There is specifically no inconsistency with the λ -scaling found in the previous chapter that were based on a fixed threshold for the entire λ range. We comment on this point in more detail in appendix E, where we also perform a fit in which the same threshold is used for all values of λ . Finally, we want to emphasize that part of the deviation from a perfect logarithmic relation for $\lambda = 1.2$ originates from setting the maximal occupation per mode $C < N$.

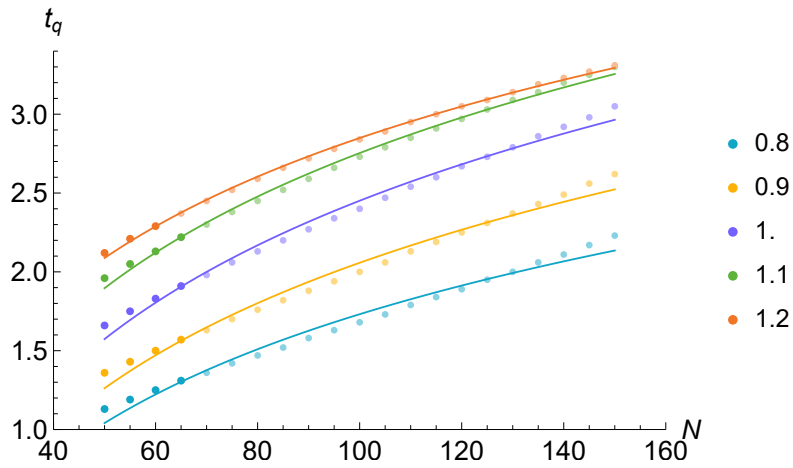
¹⁷For sufficiently small c , one can approximate

$$ax^c + b = a(1 + c \ln x + O((c \ln x)^2)) + b. \quad (4.26)$$

Thus, only keeping the term linear in $\ln x$ is a good approximation as long as $c \ln x \ll 1$ for the largest value of x under consideration. Since we scan up to $N = 150$, the critical value of c is $1/\ln 150 \sim 0.2$.



(a) Linear fits.



(b) Logarithmic fits.

Figure 10: Quantum break-time as a function of N for various λ interpolating between the undercritical regime, $\lambda < 1$, and the overcritical phase, $\lambda > 1$. Linear fits in fig. 10a and logarithmic fits in fig. 10b on the same data. While for low collective coupling λ linear fits perform better, a log N dependence describes the scaling more accurately for higher λ . The break-time interpolates continuously between a linear regime and a logarithmic one. Note that the increase in the break-time for higher λ is caused by an adjusted threshold for each λ .

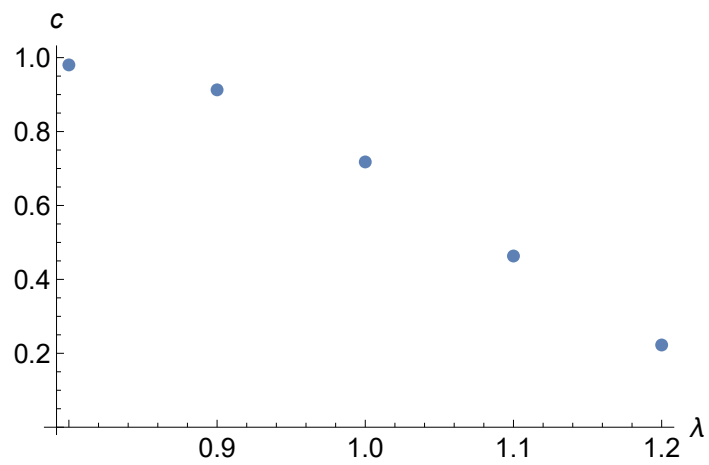


Figure 11: Numerical values of exponent fit parameter c of a polynomial fit (see eq. (4.9)).

5 Conclusion

5.1 Summary of findings

A classical description generically represents an approximation of a more fundamental theory that includes quantum effects. In this paper, we have investigated the quantum break-time t_q , after which the classical approximation breaks down. To this end, we have developed further the system [10, 32] to construct a new prototype model (NPM) defined in eq. (3.6). It can be characterized by two parameters in addition to the particle number N . The first one is the collective coupling $\lambda = \alpha N$, where α sets the strength of elementary quantum interactions. We can normalize λ such that the system exhibits a classical instability for $\lambda > 1$. The other parameter corresponds to the number Q of dynamically accessible quantum modes.

After deriving analytic estimates, we have employed the software *TimeEvolver* [108] to numerically compute full quantum dynamics. While detailed results are displayed in the main part, a simplified summary of our findings reads as follows: In the generic case in which the system is classically stable, quantum breaking only takes place if Q is sufficiently large. In this case, the dependence on the particle number is linear, $t_q \sim N$. In contrast, the regime $\lambda > 1$, in which a classical instability is present, causes a breakdown of the classical description for all values of Q . If the number of modes is not too large, $Q \ll N$, we get the timescale $t_q \sim \ln N$ whereas a large Q implies

$$t_q \sim \sqrt{N}. \quad (5.1)$$

Finally we have investigated the transition region $\lambda \approx 1$ and found

$$t_q \sim N^\gamma, \quad (5.2)$$

where $0 < \gamma < 1$. The scaling (5.2) smoothly interpolates between the linear scaling corresponding to $\lambda \ll 1$ and the logarithmic dependence caused by $\lambda \gg 1$. In particular, we also observed the scaling (5.1) close to the critical value $\lambda = 1$.

Moreover displaying the dependencies on Q and λ , we can schematically summarize the above discussion,

$$t_q \sim \begin{cases} \frac{N}{Q\lambda^2} & \lambda \ll 1 \\ \frac{\ln N}{Q\sqrt{\lambda-1}} & \lambda \gg 1 \ \& \ Q \ll N \\ \sqrt{N}f_1(Q, \lambda) & \lambda \gg 1 \ \& \ Q \gg N \\ N^\gamma f_2(Q, \lambda) & \text{otherwise} \end{cases}, \quad (5.3)$$

where $0 < \gamma < 1$ and $f_1(Q, \lambda)$, $f_2(Q, \lambda)$ are functions of Q and λ . For fixed Q , all scalings shown in eq. (5.3) are compatible with the classical limit. In terms of classical quantities, namely the total energy E and the elementary frequency ω of (free) oscillations, the number of particles scales as $N \sim E/(\hbar\omega)$ (see [45, 49]). Consequently, the classical limit $\hbar \rightarrow 0$ leads to $N \rightarrow \infty$ and $t_q \rightarrow \infty$, i.e., the classical approximation never breaks down.

However, there is an important caveat regarding quantum breaking in the undercritical regime. We have found indications that in this case quantum breaking is only possible if $Q \gtrsim N$. As is evident from the first line of eq. (5.3), this would imply that $1 > t_q \sim \hbar^0$, corresponding to an essentially instantaneous breakdown of the classical approximation. Thus, no classical description exists to begin with and so it becomes meaningless to search for its breakdown. Should this finding be confirmed, then the following far-reaching statement about our model would be true: *If there is no classical instability and a viable classical description exists at some initial time, then this classical description remains valid indefinitely.* Evidently, such a finding could shed light on the long-standing question why a complete deviation from the classical approximation is such a rarely observed phenomenon.

Several questions remain to be answered. While we have provided heuristic derivations for the first two lines of eq. (5.3), such an analytic argument is missing in the other cases. In particular, it would be interesting to better understand how the scaling $t_q \sim \sqrt{N}$ arises. Moreover, we have only established when the classical description ceases to be valid but not what exactly happens at this point. As a next step, we are currently investigating signatures of a deviation from the classical approximation, e.g., related to higher point functions [162]. Most of all, it remains to be determined if our results also apply to other systems. This is especially important in the regimes that we have for the first time observed dynamically, such as the scaling (5.1), as well as for the question if quantum breaking may become impossible in the absence of a classical instability. Evidently, systems that are experimentally realizable are of special interest¹⁸.

5.2 Outlook: connection to gravity

In this work, we have developed further the system [10], which originated from the quantum N-portrait of a black hole [26]. In this microscopic model that we reviewed in section 1.2, a black hole of mass M consists of $N = G_N M^2 / \hbar$ soft gravitons of wavelength $r_g = 2G_N M$, where G_N is Newton's constant and r_g corresponds to the Schwarzschild radius. Since the individual gravitational coupling is $\alpha = \hbar G_N / r_g^2$, the system finds itself at the critical point, $\lambda = 1$. An analogous microscopic model exists for the expanding de Sitter spacetime [49, 56]. In this case, the Hubble rate H determines the number of gravitons, $N = 1 / (\hbar G_N H^2)$, and the gravitational interaction strength, $\alpha = \hbar G_N H^2$. Again we have $\lambda = 1$. In summary, criticality emerges as a crucial property of both black holes and de Sitter.

Therefore, one may be able to gain information about gravity by studying our NPM for $\lambda = 1$. In this case, we observed $t_q \sim N^\gamma$, with $\gamma \approx 1/2$. Combining this finding with similar

¹⁸For example, the Hamiltonian eq. (3.6) can also be thought of as originating from a multi-component or spinor BEC [163, 164]. In a spinor condensate, the various k -modes could label different magnetic sub-levels m where $-J \leq m \leq J$ with total angular momentum J . In the absence of an external magnetic field, the different spin modes have identical kinetic terms while their interactions can be modeled by the same term structure as in eq. (3.6) in the condensate phase as long as only the lowest momentum mode is excitable (see [165] for a review of spinor BECs). Spinor condensates with a similar number of (nearly)-degenerate modes as considered in this study are already experimentally accessible, e.g., for $J = 8$ [166] or for $J = 6$ [167].

results in other systems [41, 63], we are tempted to speculate that the quantum break-times for black holes and de Sitter could be

$$t_q \stackrel{?}{\sim} \sqrt{N} r_g, \quad t_q \stackrel{?}{\sim} \sqrt{N} H^{-1}. \quad (5.4)$$

These timescales are much shorter than Page’s time [120], which corresponds to a scaling $t_q \sim N$. If the classical description broke down as early as shown in eq. (5.4), this would have far-reaching consequences for cosmology. Observational constraints on primordial black holes can change radically and small primordial black holes below 10^{15} g could become viable dark matter candidates [64] (see also [168]). Moreover, new observables emerge in the early Universe that are sensitive to the whole history of inflation [63].

Evidently, it is important to construct analogue models that share more properties with black holes or expanding spacetime than our NPM. Imitating information-processing characteristics [10, 28] appears to be a particularly fruitful avenue; see [64] for a concrete proposal. The analogies of gravity with much simpler non-relativistic systems open up an intriguing prospect of answering long-standing questions about black holes and de Sitter in table-top experiments. Analogue models that focus on geometry have already been realized experimentally both for black holes [169–171] and for cosmology [172–176] (see also [177]). It would be exciting to devise laboratory systems that implement an analogy to gravity based on criticality and information processing.

Acknowledgments

We thank Gia Dvali, Rina Kanamoto and Hiroki Saito for extremely useful discussions and insightful feedback. We are grateful to Michael Gedalin and Shira Chapman for granting us access to their HPC resources. The work of M.M. was supported by a Minerva Fellowship of the Minerva Stiftung Gesellschaft für die Forschung mbH and in part by the Israel Science Foundation (grant No. 741/20) and by the German Research Foundation through a German-Israeli Project Cooperation (DIP) grant “Holography and the Swampland”. S.Z. acknowledges support of the Fonds de la Recherche Scientifique - FNRS.

A Bound on self-coupling

In the analytic consideration of section 3, we neglected the effect of C_m . In the following, we shall study under which conditions this is justified. As before, we shall apply the Bogoliubov-approximation, $\hat{a}_0 \approx \sqrt{N - \Delta N}$, where ΔN is the number of particles that are not in the \hat{a}_0 -mode, i.e., we immediately took into account backreaction. Up to corrections of order

$1/(N - \Delta N)$, we obtain from eq. (3.6):

$$\hat{H} \approx \sum_{k=1}^Q \left(\left(1 - \frac{1}{2} \lambda \left(1 - \frac{\Delta N}{N} \right) \right) \hat{n}_k - \frac{1}{4} \lambda \left(1 - \frac{\Delta N}{N} \right) (\hat{a}_k^2 + \hat{a}_k^{\dagger 2}) \right) \quad (\text{A.1a})$$

$$+ \frac{C_m}{2} \sum_{k=1}^Q \sum_{\substack{l=1 \\ l \neq k}}^Q f(k, l) (\hat{a}_k^{\dagger 2} \hat{a}_l^2 + \text{h.c.}) . \quad (\text{A.1b})$$

For the sake of the following consideration, we neglected corrections that scale with α but kept all terms involving C_m . Subsequently, we shall use two distinct arguments.

Following a similar reasoning as in [64, 178], we can evaluate the expectation value of the Hamiltonian (A.1). We get approximately

$$\langle \hat{H} \rangle = \sum_{k=1}^Q \left(1 - \lambda \left(1 - \frac{\Delta N}{N} \right) \right) \Delta N + 2C_m \Delta N . \quad (\text{A.2})$$

Here we took into account that due to $f(k, l)$, summing N_Q^2 entries with both positive and negative signs leads to a contribution on the order of N_Q (see e.g., [179] and [64] where an analogous argument was used).¹⁹ Now we impose the requirement that the sign of $\langle \hat{H} \rangle > 0$ should not change because of the inclusion of C_m . This amounts to imposing that the additional coupling does not alter the under- or overcriticality of the system. Applying this condition to eq. (A.2) leads to the mild bound

$$|C_m| \lesssim \frac{1 - \lambda}{2} . \quad (\text{A.3})$$

Next, we consider a second line of argument, which is only applicable in the undercritical case $\lambda < 1$. First, we consider two species, $Q = 2$ and then eq. (A.1) gives

$$\hat{H} = \sum_{k=1}^2 \left(\left(1 - \frac{1}{2} \lambda \left(1 - \frac{\Delta N}{N} \right) \right) \hat{n}_k - \frac{1}{4} \lambda \left(1 - \frac{\Delta N}{N} \right) (\hat{a}_k^2 + \hat{a}_k^{\dagger 2}) \right) - \frac{C_m}{2} (\hat{a}_1^{\dagger 2} \hat{a}_2^2 + \text{h.c.}) , \quad (\text{A.4})$$

where we replaced the effect of $f(k, l)$ by a negative sign since in this case its effect is maximal, as is evident from the subsequent calculation. Focusing on the \hat{a}_1 -mode, we will momentarily also assume that \hat{a}_2 is macroscopically occupied and approximate $\hat{a}_2 \approx \sqrt{\Delta N/2}$, where $N \gg \Delta N \gg 1$.

Then we get

$$\hat{H}|_{k=1} = \left(1 - \frac{1}{2} \lambda \left(1 - \frac{\Delta N}{N} \right) \right) \hat{n}_1 - \frac{1}{2} \left(\frac{1}{2} \lambda \left(1 - \frac{\Delta N}{N} \right) + \frac{C_m \Delta N}{2} \right) (\hat{a}_1^2 + \hat{a}_1^{\dagger 2}) \quad (\text{A.5})$$

$$= \mathcal{E} \hat{n}_1 - \frac{g}{2} (\hat{a}_1^2 + \hat{a}_1^{\dagger 2}) , \quad (\text{A.6})$$

¹⁹If e.g., ΔN particles are distributed over $Q > \Delta N$ modes with 2 particles per mode, we get $(\Delta N/2)^2$ non-zero entries and $\langle \sum_{k=1}^Q \sum_{\substack{l=1 \\ l \neq k}}^Q f(k, l) (\hat{a}_k^{\dagger 2} \hat{a}_l^2 + \text{h.c.}) \rangle \approx \sqrt{(\Delta N/2)^2} \cdot 4 \cdot 2 = 4\Delta N$.

where we defined

$$\mathcal{E} = 1 - \frac{1}{2}\lambda \left(1 - \frac{\Delta N}{N}\right), \quad g = \frac{\lambda \left(1 - \frac{\Delta N}{N}\right) + C_m \Delta N}{2}. \quad (\text{A.7})$$

Correspondingly, we choose the coefficients in the Bogoliubov transformation (2.12) as

$$u^2 = \frac{1}{2} \left(\frac{\mathcal{E}}{\epsilon} + 1\right), \quad v^2 = \frac{1}{2} \left(\frac{\mathcal{E}}{\epsilon} - 1\right), \quad (\text{A.8})$$

where now

$$\epsilon = \sqrt{\mathcal{E}^2 - g^2}. \quad (\text{A.9})$$

As before, the Hamiltonian becomes

$$\hat{H} = \epsilon \hat{n}^b. \quad (\text{A.10})$$

Plugging the definitions (A.7) in ϵ , we get

$$\epsilon = \sqrt{\left(1 - \frac{1}{2}\lambda \left(1 - \frac{\Delta N}{N}\right)\right)^2 - \left(\frac{\lambda \left(1 - \frac{\Delta N}{N}\right) + C_m \Delta N}{2}\right)^2}. \quad (\text{A.11})$$

Now we require that the \hat{a}_1 -mode does not become gapless due to C_m . This leads to

$$|C_m| \lesssim \frac{2(1 - \lambda \left(1 - \frac{\Delta N}{N}\right))}{\Delta N}. \quad (\text{A.12})$$

Finally, we can wonder how this bound change if we couple \hat{a}_1 to many hardly-occupied modes Q instead of one highly-occupied one. In this case, we need to take into account the effect of alternating signs in the coupling of the mode. Employing the same argument as in [64], we therefore replace $\Delta N/2$ by $\sqrt{\Delta N}$ to arrive at the bound:

$$|C_m| \lesssim \frac{1 - \lambda \left(1 - \frac{\Delta N}{N}\right)}{\sqrt{\Delta N}}, \quad (\text{A.13})$$

Minimizing eq. (A.13) with respect to ΔN and imposing $\Delta N \lesssim N/2$, we get $\Delta N = N \min(1/2, 1/\lambda - 1)$. This leads to²⁰

$$|C_m| \lesssim \begin{cases} \sqrt{3\alpha}(1 - \frac{\lambda}{2}) & \lambda \leq \frac{2}{3} \\ 2\sqrt{\alpha}(1 - \lambda) & \lambda > \frac{2}{3} \end{cases}. \quad (\text{A.14})$$

This indicates that $|C_m|$ can be as large as $\sqrt{\alpha}$, provided that λ is not too close to 1. This reasoning, however, is only applicable to the undercritical case $\lambda < 1$. Since ΔN is generically bigger for $\lambda > 1$, one could expect that a sharper bound is required such as $|C_m| \lesssim \alpha$.

²⁰In the above reasoning, we did not consider the effect a many unoccupied modes, i.e., the case $Q \gg N_Q$. For such parameters, one could replace $\sqrt{N_Q}$ by \sqrt{Q} in eq. (A.13). Then the sharpest bound would arise close to $\Delta N = 0$, which implies $|C_m| \lesssim \frac{1-\lambda}{\sqrt{Q}}$.

B Undercritical regime

In the following, we show plots containing data as well as fits for the individual scalings, where the main results were already presented in section 4. We start with the undercritical phase defined by $\lambda < 1$. Unless stated otherwise, we use eq. (4.4) as base value for all scans in this section and we show the parameter values again for convenience:

$$\lambda = 0.8, \quad N = 50, \quad C_m = 0.016, \quad C = 4, \quad Q = 10. \quad (\text{B.1})$$

We will use three types of fitting function throughout this and the next sections. These have already been introduced in section 4 and we repeat them here for completeness:

$$\begin{aligned} \text{linear:} & & t_q &= m \cdot x + n, \\ \text{polynomial:} & & t_q &= a \cdot x^c + b, \\ \text{logarithm:} & & t_q &= p \cdot \log(x) + q, \\ \text{Shifted polynomial:} & & t_q &= \tilde{a} \cdot (x - \tilde{d})^{\tilde{c}}. \end{aligned}$$

Dependence on N In addition to the N -scan presented in the main text, we perform several others in order to verify the generality of the results. We explained above that the length of a scan interval is limited by the possibility to find an adequate threshold defining the break-time for all values within the range. Fitting over too large interval results in a meaningless definition of quantum breaking. However, it is of course valid to consider subsets of a larger interval and determine a threshold and perform fits on each of those individually. Therefore, to show that the scaling eq. (4.8) holds generically, we perform similar scans over two additional N -ranges. Besides the range presented in the main text, we also scan over a range with smaller particle number $N \in [10, 50]$ and one with larger one $N \in [1000, 5000]$. We perform a linear as well as a polynomial fit, which yields the following fitting parameters:

$$\begin{aligned} \text{linear fit :} & \quad m = 0.027, \quad n = 0.55, \\ \text{polynomial fit :} & \quad a = 0.048, \quad b = 0.44, \quad c = 0.87, \\ & \quad \text{for } N \in [10, 50], \quad C_m = 0.08, \end{aligned} \quad (\text{B.2})$$

as well as

$$\begin{aligned} \text{linear fit :} & \quad m = 0.00032, \quad n = 0.5, \\ \text{polynomial fit :} & \quad a = 0.0003, \quad b = 0.5, \quad c = 1.0, \\ & \quad \text{for } N \in [10^3, 5 \cdot 10^3], \quad C_m = 8 \cdot 10^{-4}. \end{aligned}$$

Fits for both ranges are depicted in figs. 12a and 12b and we observe a clear linear dependency in both cases. That the smaller N -range deviates more from a perfect linear relation can be explained by $1/N$ effects due to the small particle number. Besides that the numerical values for the fit are quantitatively very similar. Apart from the non-trivial threshold fixing, one fitting function could in principle be valid over several orders of magnitude in N .

To study the impact of our artificial parameter C , we repeat the study from 4.2 with a higher capacity $C = 6$ over the same set of parameters. The data and fit can be found in fig. 12c with fitting values given by

$$\begin{aligned} \text{linear fit :} & \quad m = 0.0065, \quad n = 0.56, \\ \text{polynomial fit :} & \quad a = 0.012, \quad b = 0.46, \quad c = 0.90, \\ & \quad \text{for } C = 6. \end{aligned}$$

Finally, we also want to take a close look at the influence of C_m . In the following, we will set $C_m = 0$ and verify that this yields the same result. We vary the total particle number between $50 \leq N \leq 250$ and apart from setting the interspecies coupling to zero, we keep all other parameters as used in eq. (B.1). This yields

$$\begin{aligned} \text{linear fit :} & \quad m = 0.006, \quad n = 0.5, \\ \text{polynomial fit :} & \quad a = 0.0074, \quad b = 0.47, \quad c = 0.97, \\ & \quad \text{for } C_m = 0. \end{aligned}$$

A exponent c close to one again indicates a linear relation. The corresponding plot is depicted in fig. 12d. Summarizing, a linear relation between particle number N and the break-time t_q is observed for all considered parameter choices.

Dependence on Q We perform two Q -scans. The first one has total occupation number $N = 50$ as set by eq. (4.4) and this scan is also discussed in the main section 4. Additionally, we also perform a second one with $N = 10$ (and adjusted C_m). The data for both scans are plotted in figs. 13a and 13b, respectively. A polynomial fit of the form eq. (4.9) yields:

$$\begin{aligned} a = 6.57, \quad b = 0.48, \quad c = -0.99 & \quad \text{for } N = 50, C_m = 0.016. \quad (\text{B.3}) \\ a = 12.25, \quad b = 0.40, \quad c = -1.00 & \quad \text{for } N = 10, C_m = 0.08, \end{aligned}$$

Both values are very close to the analytic expected value of $c = -1$. However, we have to stress that these values vary when changing the fitting range in fig. 13. Especially including smaller Q in the fit leads to an increase in the numerical value of the exponent. This can partly be attributed to the difficulty of finding a meaningful threshold for a large parameter interval. However, some uncertainty seems to exist when fitting Q and extracting numerical fit values. Apart from this we find that the fitting values, especially the exponent c , vary over the same interval independent of the particular N . We conclude that the observed Q -scaling is stable against the change of the variable N .

Dependence on λ Starting from the base values (4.4), we vary the collective coupling in this paragraph within the range $0.2 \leq \lambda \leq 0.9$. However, as mentioned several times by now, fitting over too large intervals is problematic due to inadequate thresholds. For this reason we split the interval in two subintervals and perform a fit on each section separately. The

first one is defined by $0.2 \leq \lambda \leq 0.5$, the second one by $0.5 \leq \lambda \leq 0.9$. The data and fit can be found in fig. 14a and fig. 14b respectively. The detail fit parameters are given by

$$\begin{aligned} a = 0.059, \quad b = 0.22, \quad c = -1.76 & \quad \text{for} \quad 0.2 \leq \lambda \leq 0.5, \\ a = 0.22, \quad b = 0.41, \quad c = -2.26 & \quad \text{for} \quad 0.5 \leq \lambda \leq 0.9. \end{aligned} \quad (\text{B.4})$$

Again the exponent c shows fluctuations when fitting over different values. This can probably again be traced to threshold effects. The fitting parameters for the exponent on the two different intervals seem to spread around the analytical estimated scaling of $t_q \sim 1/\lambda^2$.

Dependence on C_m As explained in the main text, we do not expect C_m to play a major role over the value range that we consider. To check this expectation on the concrete system, we again perform numerical simulation while varying the interspecies coupling over the range $0 \leq C_m \leq 0.5$. Again we use eq. (4.4) as base values for the parameters of the system. The data is plotted in fig. 14c. It is clear from the plot that there is only a marginal dependence of the break-time on C_m despite the fact we vary C_m to much larger values than we consider in the remainder of this paper. We therefore do not perform a fit. It is however interesting to note that in the undercritical phase there exist two different regimes. In the first one, increasing C_m leads to a reduction of the break-time while going beyond a certain value ($C_m \sim 0.24$ in this specific instance) the break-time increases and departure from the initial state takes a longer period of time.

C Overcritical regime with few species

Next we show data and fits for the overcritical phase with $\lambda > 1$. This phase can be categorized in two regimes according to section 3. We follow the same order as in the main part and start with the case when Q is small compared to the number of total particles N , corresponding to the first case in eq. (3.16). Unless stated otherwise, all scans in this section take eq. (4.13) as their base values. which we print again for convenience:

$$\lambda = 1.2, \quad N = 50, \quad C_m = 0.016, \quad C = 50, \quad Q = 3. \quad (\text{C.1})$$

Dependence on N The main scan about the N -dependency of the break time is in full detail presented in the main text in section 4.3. In addition to the one shown there, we perform here a simulation with higher capacity $C = 60$ and vanishing interspecies coupling $C_m = 0$. Besides these changes, the scan range $50 \leq N \leq 250$ as well as the remaining parameters (see eq. (4.13)) are kept the same. The data and fit for higher capacity can be found in fig. 15b, those for $C_m = 0$ are presented in fig. 15a. Fitting a logarithmic function of the form eq. (4.14) to both sets yields the following parameters:

$$\begin{aligned} p = 1.18, \quad q = -2.25 & \quad \text{for} \quad C_m = 0, \\ p = 1.21, \quad q = -2.22 & \quad \text{for} \quad C = 60. \end{aligned} \quad (\text{C.2})$$

In all three sets (base, higher C , vanishing C_m), the values for the fit parameters are very similar and verify the robustness of our numerical findings. Notice, however, although the fits are very similar the precise break-times are different.

Dependence on Q We run simulation with varying the species number within $2 \leq Q \leq 8$. The data, which is concisely summarized in section 4.3, can be reviewed in more detail in fig. 16a. Moreover, the precise fitting values are given by

$$a = 4.39, \quad b = 0.78, \quad c = -0.84. \quad (\text{C.3})$$

Again we observe a minor deviation from the analytic expectation $t_q \sim 1/Q$. We have to emphasize that the precise values for the above fit depend on the range one fits. In summary, although the precise numerical values are model dependent, they still seem near the analytic expectation within numerical uncertainties.

Dependence on λ The data for the λ scan presented in the main text can be found in fig. 16b. As discussed previously, it can be described very accurately by a shifted polynomial function defined in eq. (4.17). The fit yields following values:

$$\tilde{a} = 1.24, \quad \tilde{d} = 0.88, \quad \tilde{c} = -0.49. \quad (\text{C.4})$$

The data and the fit are visualized in fig. 16b.

Dependence on C_m Completely analogously to the undercritical phase, the break-time should not depend on C_m significantly. We test this claim again by scanning of $0.01 \leq C_m \leq 0.09$. The data can be found in fig. 16c. As expected, there is only a marginal influence of C_m on the break-time in the range of values considered. Note that the threshold determined by the smallest amplitude in this scan seems inadequate for the dynamics with high amplitudes for larger coupling constant $C_m \gtrsim 0.08$. However, the qualitative behavior seems to be unaffected by this choice, as it is evident from the continuous and slow change in fig. 16c.

D Overcritical regime with many species

Next, we present the data and details about the fits of section 4.4. This regime lies in the overcritical phase $\lambda > 1$ with a large number of species as compared to the total occupation number of the system. Specifically, it corresponds to the second line in eq. (3.16). As base values, we use eq. (4.19) unless states otherwise and we print them again for convenience:

$$\lambda = 1.2, \quad N = 10, \quad C_m = 0.08, \quad C = 16, \quad Q = 10. \quad (\text{D.1})$$

Dependence on N Similarly to the other overcritical regime, we check the generality of the result presented in the main section 4.4. Therefore, we again perform two additional scans with vanishing interspecies coupling C_m as well as higher capacity C . Again, we vary N within the interval $5 \leq N \leq 25$. The data and corresponding polynomial fits can be

reviewed in figs. 17a and 17b, respectively. The fit parameters have the following numerical values

$$\begin{aligned} a = 0.18, \quad b = 0.27, \quad c = 0.60 & \quad \text{for} \quad C_m = 0.0, \\ a = 0.26, \quad b = 0.21, \quad c = 0.54 & \quad \text{for} \quad C = 20. \end{aligned} \quad (\text{D.2})$$

In analogy to the other N -scans, the corresponding scalings are insensitive to the C (as long as it is chosen large enough) as well as the precise value of C_m . Specifically, the exponent of the polynomial seems to spread around the numerical value $c = 0.5$. Note that N gets very small in these scans so we expect that finite size effects can have an influence in this analysis.

Dependence on Q In order to remain in the many species regime of the overcritical phase, we have to choose Q large enough compared to N according to eq. (3.16). For this reason we will vary Q within $10 \leq Q \leq 40$ in the following. The fit and data presented in the main section can be seen in fig. 18a. In addition to the scan defined by eq. (4.4) and presented in section 4.4, we also run a scan with higher total occupation and correspondingly adjusted C_m . Due to limited computational resources, increasing the total particle number N requires to reduce the scan range to $10 \leq Q \leq 18$. We also adjust the minimal Q to compensate for the larger N to stay in the many species regime. The data and fit can be seen in fig. 18b. For both runs, we summarize the fit parameters in the following table

$$\begin{aligned} a = 4.29, \quad b = 0.098, \quad c = -0.59 & \quad \text{for} \quad N = 10, C_m = 0.08, \\ a = 5.07, \quad b = 0.12, \quad c = -0.58 & \quad \text{for} \quad N = 20, C_m = 0.04. \end{aligned} \quad (\text{D.3})$$

Dependence on λ As illustrated in eq. (5.3) we were not able to obtain a conclusive analytic understanding of the scaling of the break-time with the collective coupling λ in the overcritical phase in the presence of many accessible modes. We therefore perform several different fits over the interval $1.1 \leq \lambda \leq 1.3$. The obtained data with a shifted polynomial fit can be seen in fig. 19a. Motivated by the known critical point of quantum phase transition $\lambda = 1$ in the limit of large N we also perform a fit with fixed shift $\tilde{d} = 1$ in fig. 19b. We note that fixing the shift seems to worsen the fit. Additionally, we also show the same data with a polynomial fit in fig. 19c. The numerical values for the fit function are given by

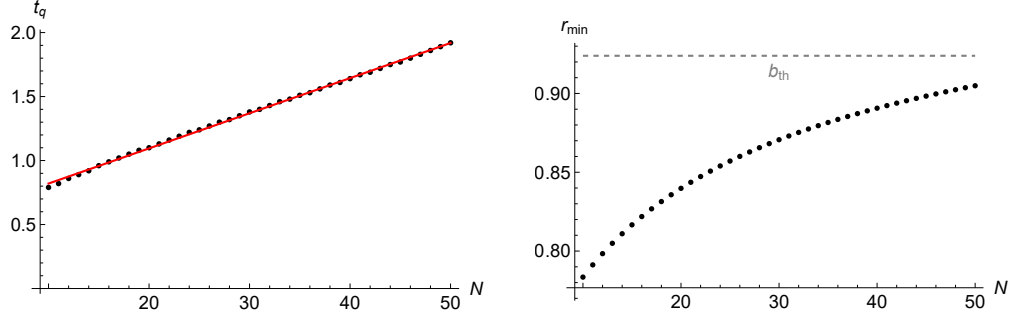
$$\begin{aligned} \tilde{a} = 0.75, \quad \tilde{d} = 0.66, \quad \tilde{c} = -0.60 & \quad \text{for function eq. (4.17),} \\ \tilde{a} = 0.78, \quad \tilde{c} = -0.21 & \quad \text{for function eq. (4.17) and fixed } \tilde{d} = 1, \\ a = 0.90, \quad b = 0.53, \quad c = -2.59 & \quad \text{for function eq. (4.9).} \end{aligned} \quad (\text{D.4})$$

The value differs more significantly from the square root indication found in the few species regime for the same fit function (4.9). We emphasize, however, that a polynomial fit with exponent $c = -2.6$ describes the data equally accurate and it is at this point not clear which (or another) scaling is the true dependency on λ .

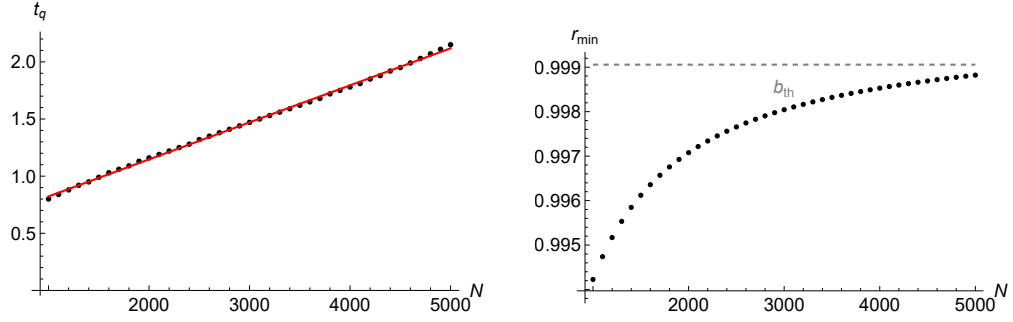
Dependence on C_m Last but not least, we perform a C_m -scan over the range $0 \leq C_m \leq 0.5$ with parameter choice (4.19). The data is visualized in fig. 18c. Similarly to the undercritical phase discussed earlier, also this regime shows no significant change over the whole interval. We therefore conclude that C_m is unimportant for the break-time in our prototype system eq. (3.6).

E Critical interpolation

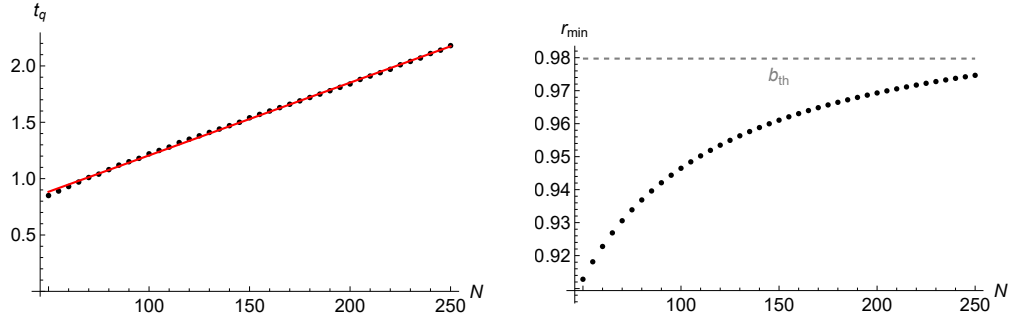
We performed several N -scans in section 4.5 to interpolate between the undercritical and overcritical (with few species) phase of system (3.6). As discussed above, the dynamics changes continuously from a linear scaling to logarithmic one. The break-time as a function of N increases for larger λ in fig. 10. This is not in contradiction with various λ -scans throughout this paper (see for example fig. 16b in section 4.3). As already explained, this is an artifact of choosing a separate threshold for each λ individually. As a last consistency check, we perform on the same data a similar analysis, however, this time we choose a single threshold for all time evolutions. The result is shown in fig. 20 and now a larger collective coupling leads to a faster break-time, in accordance with previous findings. Also here a linear fit works best for $\lambda < 1$ while the data can be more accurately described by a log fit for $\lambda > 1$ with a continuous transformation in between. However, the distinction is significantly less clear. The reason for this is that a common threshold, which is set by the smallest amplitude in the set, is unsuitable for cases in which a large maximal amplitude of n_0/N is reached.



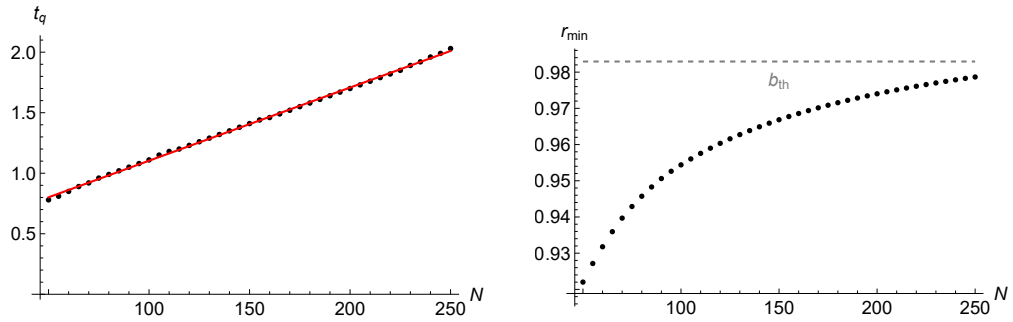
(a) N -scan with small N .



(b) N -scan with large N .

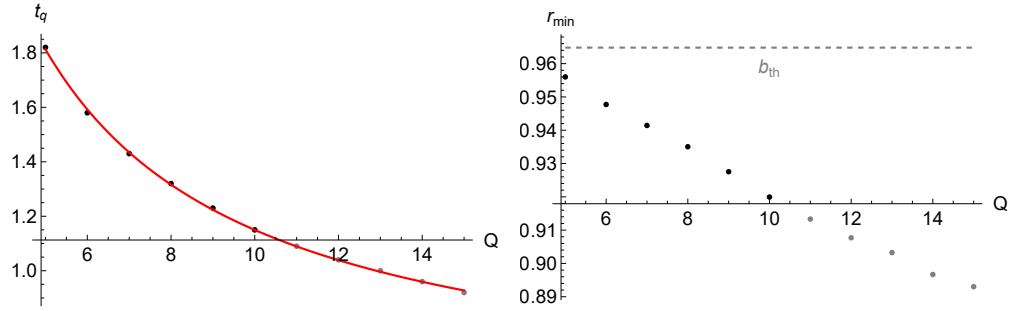


(c) N -scan with $C = 6$.

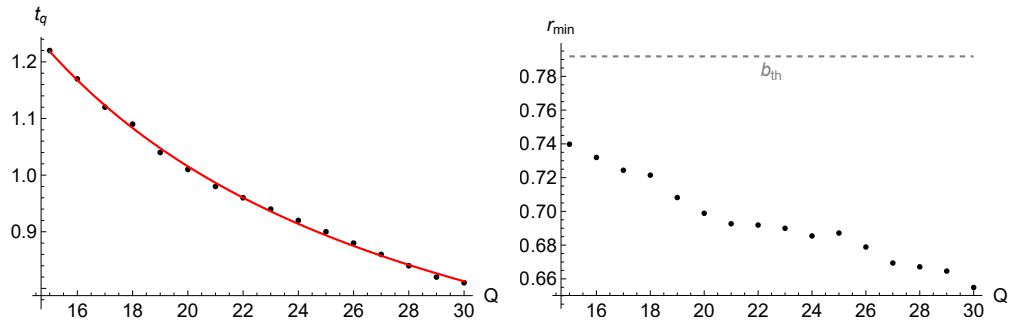


(d) N -scan with $C_m = 0$

Figure 12: Various N -Scans. **(Left)** Break-time as a function of total particle number N in the undercritical phase $\lambda < 1$. Linear fit depicted in red. Parameters given by (B.1). **(Right)** Corresponding thresholds (gray dashed line) as well as minimal occupation of the \hat{a}_0 mode.

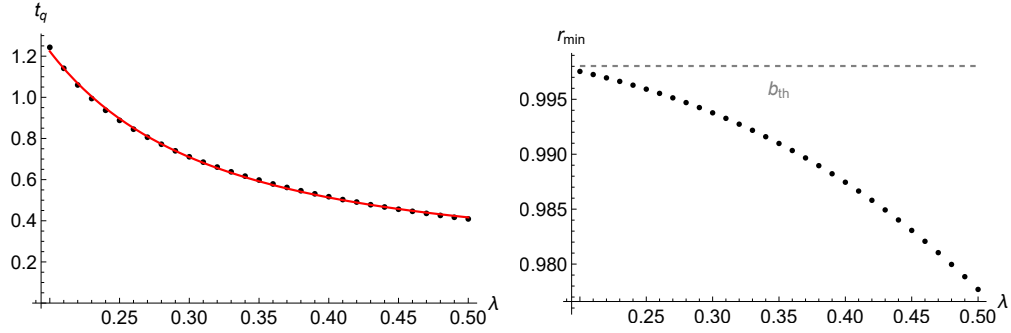


(a) Q -scan with $N = 50$.

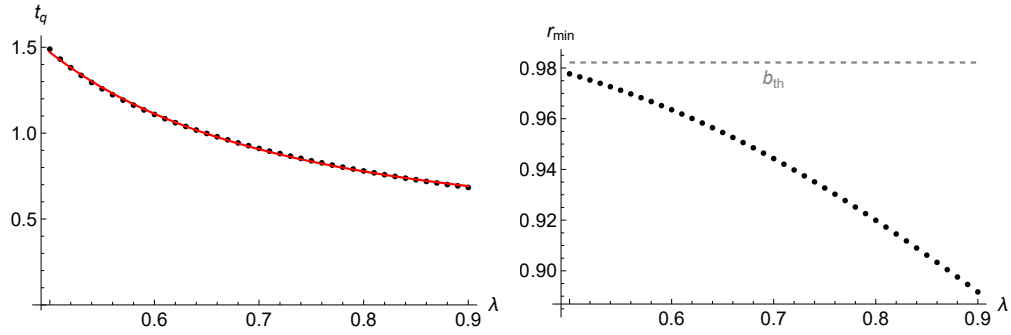


(b) Q -scan with $N = 10$.

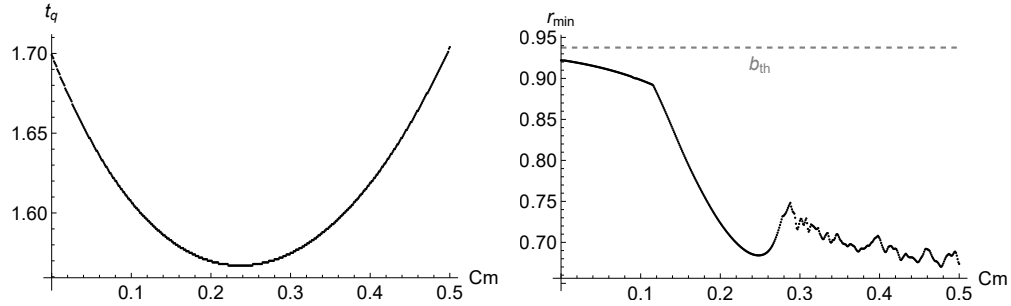
Figure 13: Various Q -Scans. **(Left)** Break-time as a function of number of species Q in the undercritical phase $\lambda < 1$. Polynomial fit depicted in red. Parameters given by (B.1). **(Right)** Corresponding thresholds (gray dashed line) as well as minimal occupation of the \hat{a}_0 mode.



(a) λ -scan with $0.2 \leq \lambda \leq 0.5$.

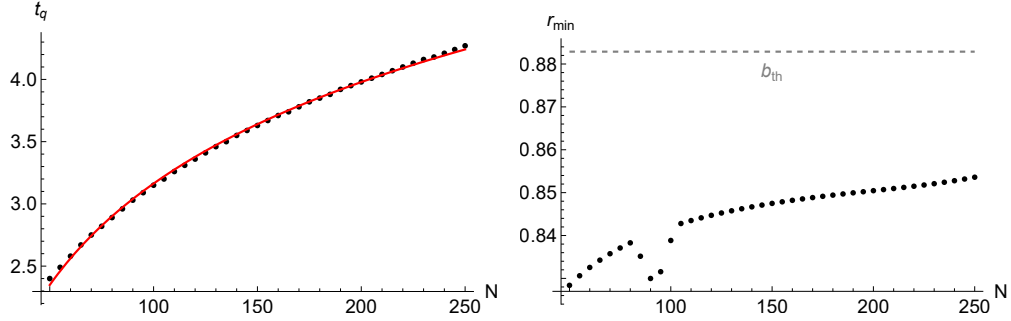


(b) λ -scan with $0.5 \leq \lambda \leq 0.9$.

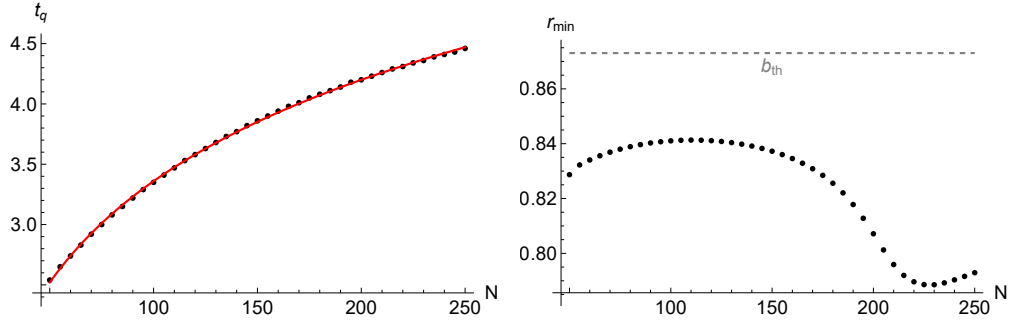


(c) C_m -Scan.

Figure 14: λ and C_m -Scans. **(Left)** Break-time as a function of number of collective coupling λ and interspecies coupling strength C_m in the undercritical phase $\lambda < 1$. Polynomial fit depicted in red. Parameters given by (B.1). **(Right)** Corresponding thresholds (gray dashed line) as well as minimal occupation of the \hat{a}_0 mode.

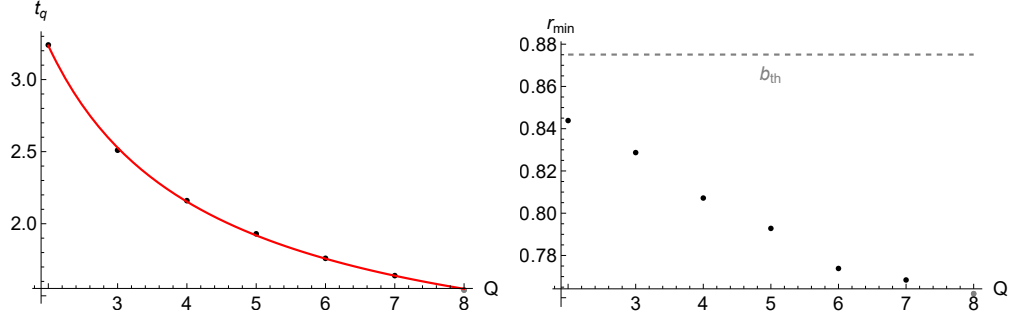


(a) N -Scan with $C_m = 0$.

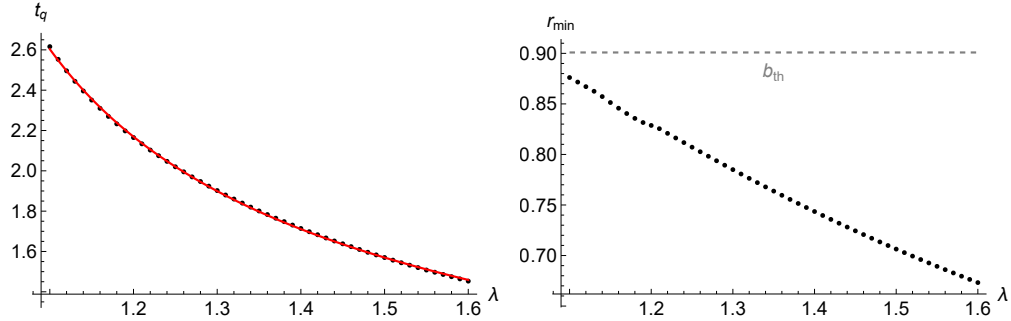


(b) N -Scan with $C = 60$.

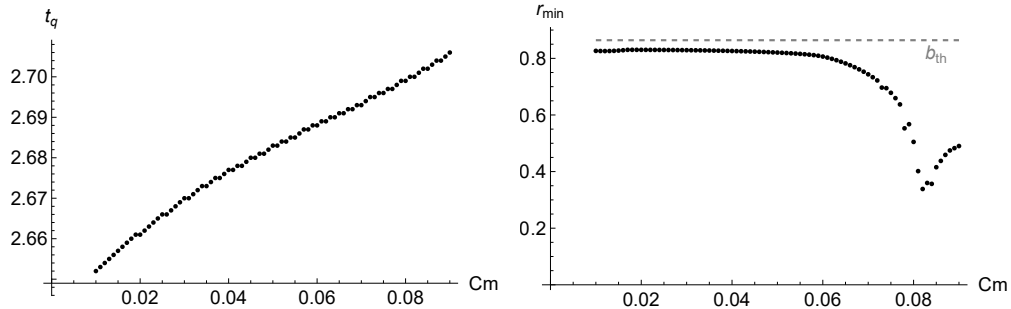
Figure 15: Various N -Scans. **(Left)** Break-time as a function of total particle number N in the overcritical phase $\lambda > 1$ with few species. Logarithmic fit depicted in red. Parameters given by (C.1). **(Right)** Corresponding thresholds (gray dashed line) as well as minimal occupation of the \hat{a}_0 mode.



(a) Q -Scan with a polynomial fit function (4.9).

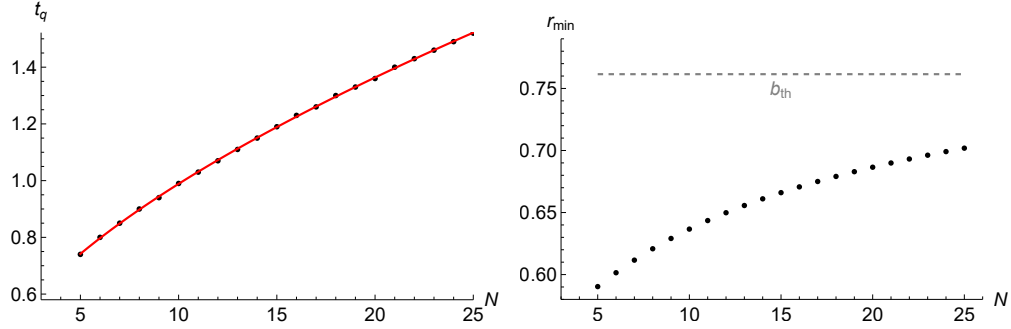


(b) λ -Scan with a shifted fit function (4.17).

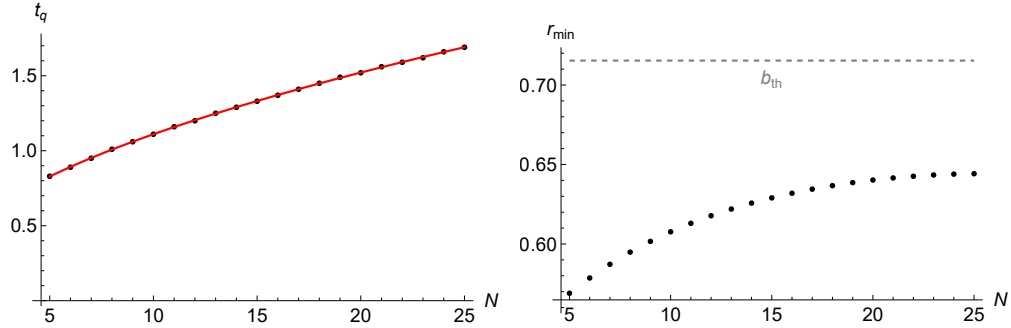


(c) C_m -Scan.

Figure 16: Q , λ and C_m -Scans. **(Left)** Break-time as a function of number of the amount of species Q , the collective coupling λ and interspecies coupling strength C_m in the overcritical phase $\lambda > 1$ with few species. (Shifted) polynomial fit depicted in red. Parameters given by (C.1). **(Right)** Corresponding thresholds (gray dashed line) as well as minimal occupation of the \hat{a}_0 mode.

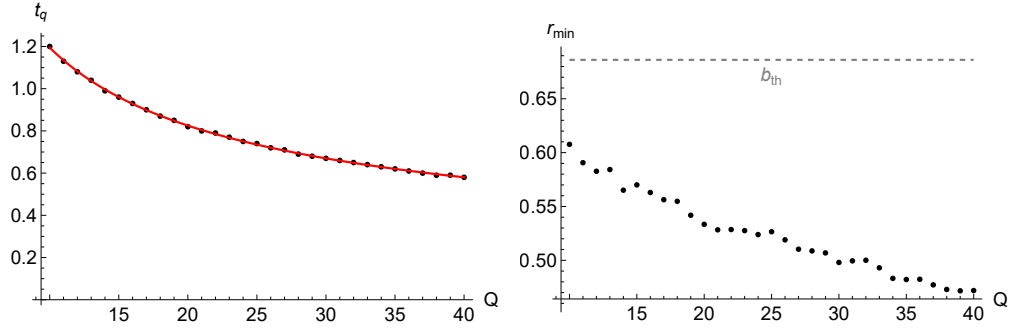


(a) N -Scan with $C_m = 0$.

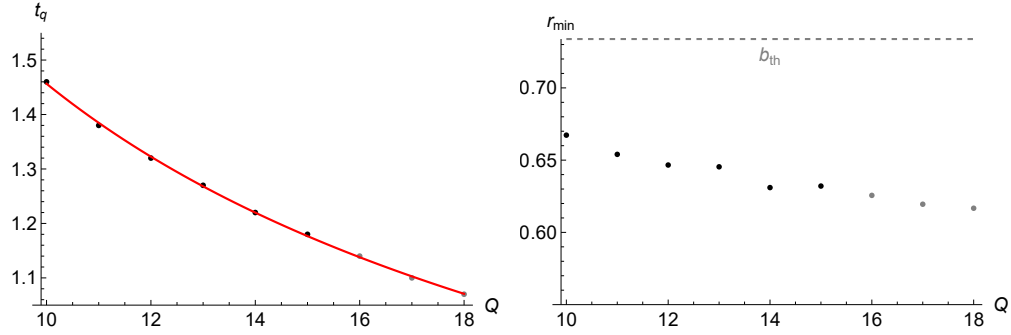


(b) N -Scan with $C = 20$.

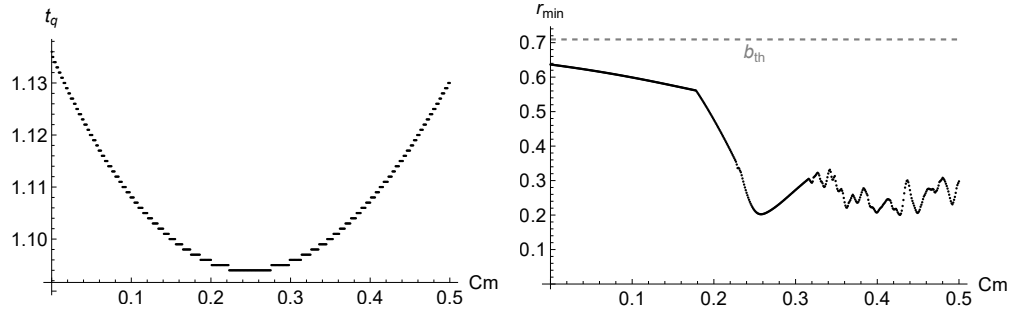
Figure 17: Various N -Scans. **(Left)** Break-time as a function of total particle number N in the overcritical phase $\lambda > 1$ with many species. Polynomial fit depicted in red. Parameters given by (D.1). **(Right)** Corresponding thresholds (gray dashed line) as well as minimal occupation of the \hat{a}_0 mode.



(a) Q -Scan with $N = 10$ and $C_m = 0.08$.

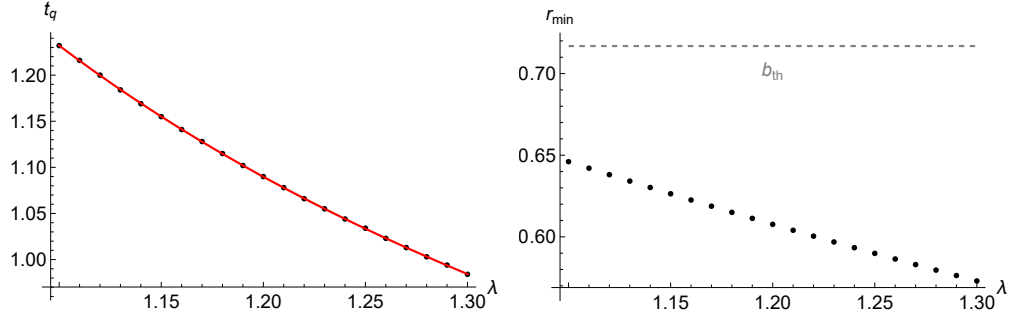


(b) Q -Scan with $N = 20$ and $C_m = 0.04$.

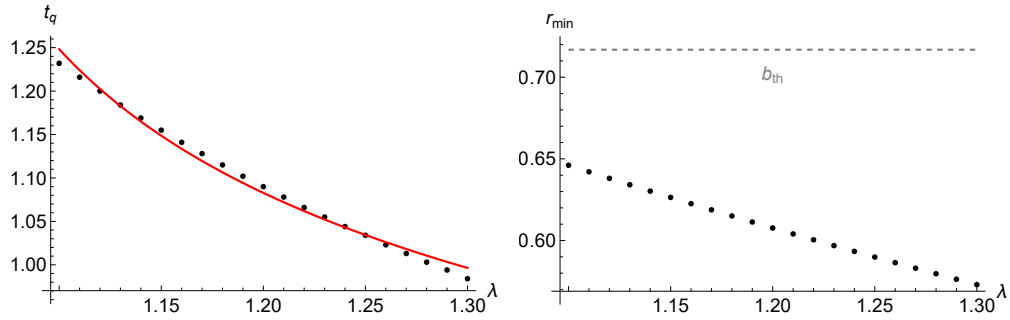


(c) C_m -Scan.

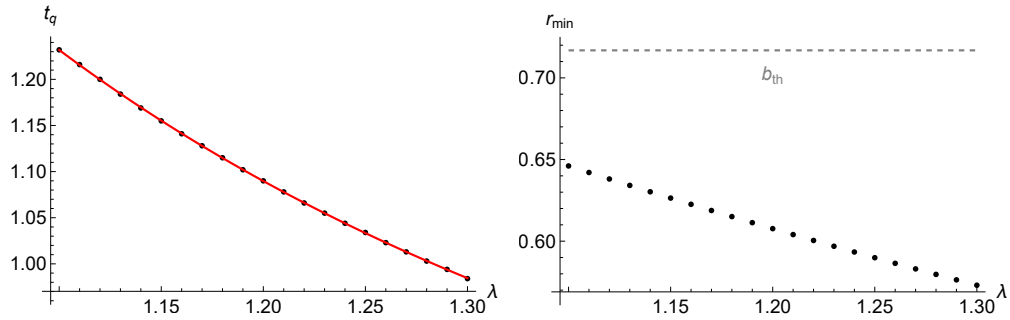
Figure 18: Q and C_m -Scans. **(Left)** Break-time as a function of number of the amount of species Q and interspecies coupling strength C_m in the overcritical phase $\lambda > 1$ with many species. (Shifted) polynomial fit depicted in red. Parameters given by (D.1). **(Right)** Corresponding thresholds (gray dashed line) as well as minimal occupation of the \hat{a}_0 mode.



(a) λ -Scan with fit function eq. (4.17).

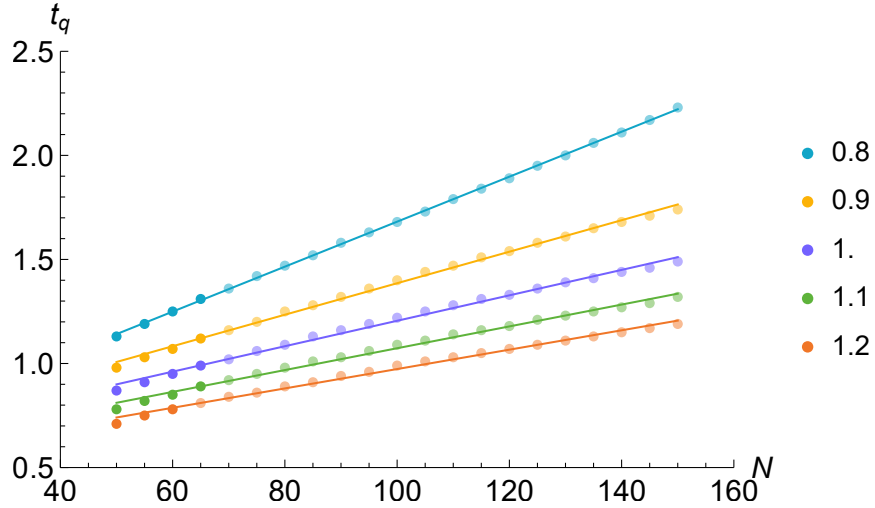


(b) λ -Scan with fit function eq. (4.17) and fixed $d = 1$.

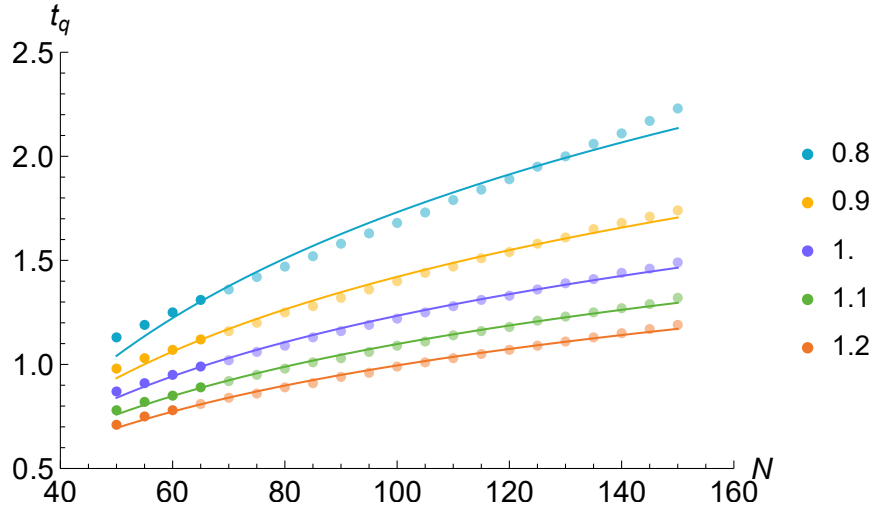


(c) λ -Scan with polynomial fit function eq. (4.9).

Figure 19: λ -Scan with different fit functions. **(Left)** Breaktime as a function of number of the amount of the collective coupling λ in the overcritical phase $\lambda > 1$ with many species. Fits depicted in red. Parameters given by (D.1). **(Right)** Corresponding thresholds (gray dashed line) as well as minimal occupation of the \hat{a}_0 mode.



(a) Linear fits.



(b) Logarithmic fits.

Figure 20: Quantum break-time as a function of N for various λ interpolating between the undercritical regime, $\lambda < 1$, and the overcritical phase, $\lambda > 1$, where a single common threshold for defining quantum breaking is used in all fits (unlike in fig. 10). Linear fits in fig. 20a and logarithmic fits in fig. 20b on the same data. Low collective coupling λ are described by a linear relation, a $\log N$ dependence describes the scaling more accurately for higher λ . Increasing the collective coupling λ leads to a faster break-time.

References

- [1] A. Einstein, *Zum Quantensatz von Sommerfeld und Epstein*, *Verh. Dt. Phys. Ges.* **19** (1917) 82.
- [2] L. de Broglie, *Remarques sur la nouvelle mécanique ondulatoire*, *C. R. Acad. Sci.* **183** (1926) 272.
- [3] L. Brillouin, *Remarques sur la mécanique ondulatoire*, *J. Phys. Radium* **7** (1926) 353.
- [4] E. Schrödinger, *Der stetige Übergang von der Mikro- zur Makromechanik*, *Naturwissenschaften* **14** (1926) 664.
- [5] P. Debye, *Die Grundgesetze der magnetischen und elektrischen Erregung vom Standpunkt der Quantentheorie*, *Phys. Z.* **27** (1926) 67.
- [6] W. Heisenberg, *Über den anschaulichen Inhalt der quantentheoretischen Kinematik und Mechanik*, *Z. Physik* **43** (1927) 172.
- [7] E. H. Kennard, *Zur Quantenmechanik einfacher Bewegungstypen*, *Z. Physik* **44** (1927) 326.
- [8] P. Ehrenfest, *Bemerkung über die angenäherte Gültigkeit der klassischen Mechanik innerhalb der Quantenmechanik*, *Z. Physik* **45** (1927) 455.
- [9] A. Einstein, *On the Quantum Theorem of Sommerfeld and Epstein*, in *The collected papers of Albert Einstein, Volume VI*, p. 434. Princeton University Press, 1997.
- [10] G. Dvali, D. Flassig, C. Gomez, A. Pritzel and N. Wintergerst, *Scrambling in the Black Hole Portrait*, *Phys. Rev. D* **88** (2013) 124041 [[1307.3458](#)].
- [11] G. Berman and G. Zaslavsky, *Condition of stochasticity in quantum nonlinear systems*, *Phys. A: Stat. Mech. and its Applications* **91** (1978) 450.
- [12] M. Berry, N. Balazs, M. Tabor and A. Voros, *Quantum maps*, *Ann. Phys.* **122** (1979) 26.
- [13] M. V. Berry, *Evolution of semiclassical quantum states in phase space*, *J. Phys. A: Math.* **12** (1979) 625.
- [14] N. L. Balazs and A. Voros, *The quantized baker's transformation*, *Europhys. Lett.* **4** (1987) 1089.
- [15] N. Balazs and A. Voros, *The quantized baker's transformation*, *Ann. Phys.* **190** (1989) 1.
- [16] M. Saraceno, *Classical structures in the quantized baker transformation*, *Ann. Phys.* **199** (1990) 37.
- [17] P. W. O'Connor and S. Tomsovic, *The unusual nature of the quantum baker's transformation*, *Ann. Phys.* **207** (1991) 218.
- [18] M. A. Sepúlveda, S. Tomsovic and E. J. Heller, *Semiclassical propagation: How long can it last?*, *Phys. Rev. Lett.* **69** (1992) 402.
- [19] S. Tomsovic and E. J. Heller, *Long-time semiclassical dynamics of chaos: The stadium billiard*, *Phys. Rev. E* **47** (1993) 282.
- [20] B. Chirikov, F. Izrailev and D. Shepelyanskij, *Dynamical stochasticity in classical and quantum mechanics*, *Sov. Sci. Rev. Sect. C* **2** (1981) 209.

- [21] B. Chirikov, F. Izrailev and D. Shepelyansky, *Quantum chaos: Localization vs. ergodicity*, *Phys. D: Nonlinear Phenom.* **33** (1988) 77.
- [22] S. N. Bose, *Plancks Gesetz und Lichtquantenhypothese*, *Z. Physik* **26** (1924) 178.
- [23] A. Einstein, *Quantentheorie des einatomigen idealen gases*, *Sitzungsber. Preuss. Akad. Wiss* **12** (1924) 261.
- [24] V. L. Ginzburg and L. D. Landau, *On the theory of superconductivity*, vol. 20. *Zh. Eksp. Teor. Fiz.*, 1950.
- [25] J. Bardeen, L. N. Cooper and J. R. Schrieffer, *Theory of superconductivity*, *Phys. Rev.* **108** (1957) 1175.
- [26] G. Dvali and C. Gomez, *Black Hole's Quantum N-Portrait*, *Fortsch. Phys.* **61** (2013) 742 [[1112.3359](#)].
- [27] G. Dvali and C. Gomez, *Black Hole's 1/N Hair*, *Phys. Lett. B* **719** (2013) 419 [[1203.6575](#)].
- [28] G. Dvali and C. Gomez, *Black Holes as Critical Point of Quantum Phase Transition*, *Eur. Phys. J. C* **74** (2014) 2752 [[1207.4059](#)].
- [29] G. Dvali and C. Gomez, *Black Hole Macro-Quantumness*, [1212.0765](#).
- [30] D. Flassig, A. Pritzel and N. Wintergerst, *Black holes and quantumness on macroscopic scales*, *Phys. Rev. D* **87** (2013) 084007 [[1212.3344](#)].
- [31] E. H. Lieb and W. Liniger, *Exact analysis of an interacting bose gas. i. the general solution and the ground state*, *Phys. Rev.* **130** (1963) 1605.
- [32] R. Kanamoto, H. Saito and M. Ueda, *Quantum phase transition in one-dimensional bose-einstein condensates with attractive interactions*, *Phys. Rev. A* **67** (2003) 013608 [[cond-mat/0210229](#)].
- [33] R. Kanamoto, H. Saito and M. Ueda, *Symmetry breaking and enhanced condensate fraction in a matter-wave bright soliton*, *Phys. Rev. Lett.* **94** (2005) 090404 [[cond-mat/0406740](#)].
- [34] R. Kanamoto, H. Saito and M. Ueda, *Critical fluctuations in a soliton formation of attractive bose-einstein condensates*, *Phys. Rev. A* **73** (2006) 033611 [[cond-mat/0511684](#)].
- [35] K. Sakmann, A. I. Streltsov, O. E. Alon and L. S. Cederbaum, *Exact ground state of finite bose-einstein condensates on a ring*, *Phys. Rev. A* **72** (2005) 033613.
- [36] A. G. Sykes, P. D. Drummond and M. J. Davis, *Excitation spectrum of bosons in a finite one-dimensional circular waveguide via the bethe ansatz*, *Phys. Rev. A* **76** (2007) 063620.
- [37] R. Kanamoto, L. D. Carr and M. Ueda, *Metastable quantum phase transitions in a periodic one-dimensional bose gas: Mean-field and bogoliubov analyses*, *Phys. Rev. A* **79** (2009) 063616 [[0901.4385](#)].
- [38] R. Kanamoto, L. D. Carr and M. Ueda, *Metastable quantum phase transitions in a periodic one-dimensional bose gas. ii. many-body theory*, *Phys. Rev. A* **81** (2010) 023625 [[0910.2805](#)].
- [39] D. Flassig, A. Franca and A. Pritzel, *Large-N ground state of the Lieb-Liniger model and Yang-Mills theory on a two-sphere*, *Phys. Rev. A* **93** (2016) 013627 [[1508.01515](#)].
- [40] G. Dvali, A. Franca, C. Gomez and N. Wintergerst, *Nambu-Goldstone Effective Theory of Information at Quantum Criticality*, *Phys. Rev. D* **92** (2015) 125002 [[1507.02948](#)].

- [41] G. Dvali and M. Panchenko, *Black Hole Type Quantum Computing in Critical Bose-Einstein Systems*, [1507.08952](#).
- [42] M. Panchenko, *The Lieb-Liniger model at the critical point as toy model for Black Holes*, [1510.04535](#).
- [43] G. Dvali and M. Panchenko, *Black Hole Based Quantum Computing in Labs and in the Sky*, *Fortsch. Phys.* **64** (2016) 569 [[1601.01329](#)].
- [44] L. Piroli and P. Calabrese, *Local correlations in the attractive one-dimensional Bose gas: From Bethe ansatz to the Gross-Pitaevskii equation*, *Phys. Rev. A* **94** (2016) 053620 [[1609.03854](#)].
- [45] G. Dvali and S. Zell, *Classicality and Quantum Break-Time for Cosmic Axions*, *JCAP* **07** (2018) 064 [[1710.00835](#)].
- [46] Q. Hummel, B. Geiger, J. D. Urbina and K. Richter, *Reversible quantum information spreading in many-body systems near criticality*, *Phys. Rev. Lett.* **123** (2019) 160401 [[1812.09237](#)].
- [47] M. Rautenberg and M. Gärttner, *Classical and quantum chaos in a three-mode bosonic system*, *Phys. Rev. A* **101** (2020) 053604 [[1907.04094](#)].
- [48] S. Zell, *The quantum substructure of gravity*, Ph.D. thesis, Munich U., 2019. [10.5282/edoc.24429](#).
- [49] G. Dvali, C. Gomez and S. Zell, *Quantum Break-Time of de Sitter*, *JCAP* **06** (2017) 028 [[1701.08776](#)].
- [50] A. Kovtun and M. Zantedeschi, *Breaking BEC*, *JHEP* **07** (2020) 212 [[2003.10283](#)].
- [51] A. Kovtun and M. Zantedeschi, *Breaking BEC: Quantum evolution of unstable condensates*, *Phys. Rev. D* **105** (2022) 085019 [[2008.02187](#)].
- [52] L. Berezghiani and M. Zantedeschi, *Evolution of coherent states as quantum counterpart of classical dynamics*, *Phys. Rev. D* **104** (2021) 085007 [[2011.11229](#)].
- [53] L. Berezghiani, G. Cintia and M. Zantedeschi, *Background-field method and initial-time singularity for coherent states*, *Phys. Rev. D* **105** (2022) 045003 [[2108.13235](#)].
- [54] H. Poincaré, *Sur le problème des trois corps et les équations de la dynamique*, *Acta Math.* **13** (1890) 1.
- [55] C. Carathéodory, *Über den Wiederkehrsatz von Poincaré*, *Sitzungsber. Preuss. Akad. Wiss* **34** (1919) 580.
- [56] G. Dvali and C. Gomez, *Quantum Compositeness of Gravity: Black Holes, AdS and Inflation*, *JCAP* **01** (2014) 023 [[1312.4795](#)].
- [57] S. Pappalardi, A. Russomanno, B. Žunkovič, F. Iemini, A. Silva and R. Fazio, *Scrambling and entanglement spreading in long-range spin chains*, *Phys. Rev. B* **98** (2018) 134303 [[1806.00022](#)].
- [58] P. Hayden and J. Preskill, *Black holes as mirrors: Quantum information in random subsystems*, *JHEP* **09** (2007) 120 [[0708.4025](#)].
- [59] Y. Sekino and L. Susskind, *Fast Scramblers*, *JHEP* **10** (2008) 065 [[0808.2096](#)].
- [60] A. Almheiri, D. Marolf, J. Polchinski and J. Sully, *Black Holes: Complementarity or Firewalls?*, *JHEP* **02** (2013) 062 [[1207.3123](#)].

- [61] S. H. Shenker and D. Stanford, *Black holes and the butterfly effect*, *JHEP* **03** (2014) 067 [[1306.0622](#)].
- [62] G. Dvali, *A Microscopic Model of Holography: Survival by the Burden of Memory*, [1810.02336](#).
- [63] G. Dvali, L. Eisemann, M. Michel and S. Zell, *Universe's Primordial Quantum Memories*, *JCAP* **03** (2019) 010 [[1812.08749](#)].
- [64] G. Dvali, L. Eisemann, M. Michel and S. Zell, *Black hole metamorphosis and stabilization by memory burden*, *Phys. Rev. D* **102** (2020) 103523 [[2006.00011](#)].
- [65] C. Dankert, R. Cleve, J. Emerson and E. Livine, *Exact and approximate unitary 2-designs and their application to fidelity estimation*, *Phys. Rev. A* **80** (2009) 012304 [[quant-ph/0606161](#)].
- [66] N. Lashkari, D. Stanford, M. Hastings, T. Osborne and P. Hayden, *Towards the Fast Scrambling Conjecture*, *JHEP* **04** (2013) 022 [[1111.6580](#)].
- [67] J. Maldacena, S. H. Shenker and D. Stanford, *A bound on chaos*, *JHEP* **08** (2016) 106 [[1503.01409](#)].
- [68] M. Blake, *Universal Charge Diffusion and the Butterfly Effect in Holographic Theories*, *Phys. Rev. Lett.* **117** (2016) 091601 [[1603.08510](#)].
- [69] J. Maldacena and D. Stanford, *Remarks on the Sachdev-Ye-Kitaev model*, *Phys. Rev. D* **94** (2016) 106002 [[1604.07818](#)].
- [70] H. Shen, P. Zhang, R. Fan and H. Zhai, *Out-of-Time-Order Correlation at a Quantum Phase Transition*, *Phys. Rev. B* **96** (2017) 054503 [[1608.02438](#)].
- [71] I. L. Aleiner, L. Faoro and L. B. Ioffe, *Microscopic model of quantum butterfly effect: out-of-time-order correlators and traveling combustion waves*, *Annals Phys.* **375** (2016) 378 [[1609.01251](#)].
- [72] S. Banerjee and E. Altman, *Solvable model for a dynamical quantum phase transition from fast to slow scrambling*, *Phys. Rev. B* **95** (2017) 134302 [[1610.04619](#)].
- [73] A. A. Patel and S. Sachdev, *Quantum chaos on a critical Fermi surface*, *Proc. Nat. Acad. Sci.* **114** (2017) 1844 [[1611.00003](#)].
- [74] A. Bohrdt, C. B. Mendl, M. Endres and M. Knap, *Scrambling and thermalization in a diffusive quantum many-body system*, *New J. Phys.* **19** (2017) 063001 [[1612.02434](#)].
- [75] D. Bagrets, A. Altland and A. Kamenev, *Power-law out of time order correlation functions in the SYK model*, *Nucl. Phys. B* **921** (2017) 727 [[1702.08902](#)].
- [76] D. Chowdhury and B. Swingle, *Onset of many-body chaos in the $O(N)$ model*, *Phys. Rev. D* **96** (2017) 065005 [[1703.02545](#)].
- [77] Y. Werman, S. A. Kivelson and E. Berg, *Quantum chaos in an electron-phonon bad metal*, [1705.07895](#).
- [78] J. Rammensee, J. D. Urbina and K. Richter, *Many-Body Quantum Interference and the Saturation of Out-of-Time-Order Correlators*, *Phys. Rev. Lett.* **121** (2018) 124101 [[1805.06377](#)].
- [79] J. Chávez-Carlos, B. López-Del-Carpio, M. A. Bastarrachea-Magnani, P. Stránský,

- S. Lerma-Hernández, L. F. Santos et al., *Quantum and Classical Lyapunov Exponents in Atom-Field Interaction Systems*, *Phys. Rev. Lett.* **122** (2019) 024101 [[1807.10292](#)].
- [80] G. Bentsen, T. Hashizume, A. S. Buyskikh, E. J. Davis, A. J. Daley, S. S. Gubser et al., *Treelike interactions and fast scrambling with cold atoms*, *Phys. Rev. Lett.* **123** (2019) 130601 [[1905.11430](#)].
- [81] C. Sünderhauf, L. Piroli, X.-L. Qi, N. Schuch and J. I. Cirac, *Quantum chaos in the Brownian SYK model with large finite N : OTOCs and tripartite information*, *JHEP* **11** (2019) 038 [[1908.00775](#)].
- [82] Z. Li, S. Choudhury and W. V. Liu, *Fast scrambling without appealing to holographic duality*, *Phys. Rev. Res.* **2** (2020) 043399 [[2004.11269](#)].
- [83] R. Belyansky, P. Bienias, Y. A. Kharkov, A. V. Gorshkov and B. Swingle, *Minimal Model for Fast Scrambling*, *Phys. Rev. Lett.* **125** (2020) 130601 [[2005.05362](#)].
- [84] B. Geiger, J. D. Urbina and K. Richter, *Emergence of a Renormalized $1/N$ Expansion in Quenched Critical Many-Body Systems*, *Phys. Rev. Lett.* **126** (2021) 110602 [[2010.08364](#)].
- [85] O. Kaikov, *Fast prescramblers*, *Phys. Rev. D* **107** (2023) 116008 [[2210.02312](#)].
- [86] C. Yin and Y. Chen, *Information scrambling of the dilute Bose gas at low temperature*, *Phys. Rev. B* **107** (2023) 054503 [[2210.03025](#)].
- [87] M. Foss-Feig, Z.-X. Gong, C. W. Clark and A. V. Gorshkov, *Nearly linear light cones in long-range interacting quantum systems*, *Phys. Rev. Lett.* **114** (2015) 157201 [[1410.3466](#)].
- [88] R.-Q. He and Z.-Y. Lu, *Characterizing many-body localization by out-of-time-ordered correlation*, *Phys. Rev. B* **95** (2017) 054201 [[1608.03586](#)].
- [89] X. Chen, T. Zhou, D. A. Huse and E. Fradkin, *Out-of-time-order correlations in many-body localized and thermal phases*, *Ann. Phys.* **529** (2017) 1600332 [[1610.00220](#)].
- [90] N. Tsuji, P. Werner and M. Ueda, *Exact out-of-time-ordered correlation functions for an interacting lattice fermion model*, *Phys. Rev. A* **95** (2017) 011601 [[1610.01251](#)].
- [91] B. Dóra and R. Moessner, *Out-of-Time-Ordered Density Correlators in Luttinger Liquids*, *Phys. Rev. Lett.* **119** (2017) 026802 [[1612.00614](#)].
- [92] I. Kukuljan, S. Grozdanov and T. Prosen, *Weak Quantum Chaos*, *Phys. Rev. B* **96** (2017) 060301 [[1701.09147](#)].
- [93] D. J. Luitz and Y. Bar Lev, *Information propagation in isolated quantum systems*, *Phys. Rev. B* **96** (2017) 020406 [[1702.03929](#)].
- [94] D. J. Luitz and Y. Bar Lev, *Emergent locality in systems with power-law interactions*, *Phys. Rev. A* **99** (2019) 010105 [[1805.06895](#)].
- [95] M. Knap, *Entanglement production and information scrambling in a noisy spin system*, *Phys. Rev. B* **98** (2018) 184416 [[1806.04686](#)].
- [96] X. Chen and T. Zhou, *Quantum chaos dynamics in long-range power law interaction systems*, *Phys. Rev. B* **100** (2019) 064305 [[1808.09812](#)].
- [97] J. Marino and A. M. Rey, *Cavity-QED simulator of slow and fast scrambling*, *Phys. Rev. A* **99** (2019) 051803 [[1810.00866](#)].

- [98] T. Zhou, S. Xu, X. Chen, A. Guo and B. Swingle, *Operator Lévy Flight: Light Cones in Chaotic Long-Range Interacting Systems*, *Phys. Rev. Lett.* **124** (2020) 180601 [[1909.08646](#)].
- [99] C. Yin and A. Lucas, *Bound on quantum scrambling with all-to-all interactions*, *Phys. Rev. A* **102** (2020) 022402 [[2005.07558](#)].
- [100] L. Colmenarez and D. J. Luitz, *Lieb Robinson bounds and out of time order correlators in a long range spin chain*, *Phys. Rev. Res.* **2** (2020) 043047 [[2005.10257](#)].
- [101] D. Wanisch, J. D. A. Espinoza and S. Fritzsche, *Information scrambling and the correspondence of entanglement dynamics and operator dynamics in systems with nonlocal interactions*, *Phys. Rev. B* **107** (2023) 205127 [[2209.09065](#)].
- [102] T. Kuwahara and K. Saito, *Absence of fast scrambling in thermodynamically stable long-range interacting systems*, *Phys. Rev. Lett.* **126** (2021) 030604 [[2009.10124](#)].
- [103] S. Xu and B. Swingle, *Scrambling Dynamics and Out-of-Time Ordered Correlators in Quantum Many-Body Systems: a Tutorial*, [2202.07060](#).
- [104] K. Richter, J. D. Urbina and S. Tomsovic, *Semiclassical roots of universality in many-body quantum chaos*, *J. Phys. A* **55** (2022) 453001 [[2205.02867](#)].
- [105] G. Dvali, *Black Holes and Large N Species Solution to the Hierarchy Problem*, *Fortsch. Phys.* **58** (2010) 528 [[0706.2050](#)].
- [106] G. Dvali and M. Redi, *Black Hole Bound on the Number of Species and Quantum Gravity at LHC*, *Phys. Rev. D* **77** (2008) 045027 [[0710.4344](#)].
- [107] G. Dvali and C. Gomez, *Quantum Information and Gravity Cutoff in Theories with Species*, *Phys. Lett. B* **674** (2009) 303 [[0812.1940](#)].
- [108] M. Michel and S. Zell, *TimeEvolver: A Program for Time Evolution With Improved Error Bound*, *Comput. Phys. Commun.* **277** (2022) 108374 [[2205.15346](#)].
- [109] S. Khlebnikov and M. Kruczenski, *Thermalization of isolated quantum systems*, [1312.4612](#).
- [110] V. K. Varma, A. Leroose, F. Pietracaprina, J. Goold and A. Scardicchio, *Energy diffusion in the ergodic phase of a many body localizable spin chain*, *J. Stat. Mech.: Theory Exp.* **2017** (2017) 053101 [[1511.09144](#)].
- [111] D. J. Luitz, N. Laflorencie and F. Alet, *Extended slow dynamical regime close to the many-body localization transition*, *Phys. Rev. B* **93** (2016) 060201 [[1511.05141](#)].
- [112] Şükrü Ekin Kocabaş, *Few-photon scattering in dispersive waveguides with multiple qubits*, *Opt. Lett.* **41** (2016) 2533 [[1603.02920](#)].
- [113] J. Rehn, A. Lazarides, F. Pollmann and R. Moessner, *How periodic driving heats a disordered quantum spin chain*, *Phys. Rev. B* **94** (2016) 020201 [[1603.03054](#)].
- [114] H. Lang, P. Hauke, J. Knolle, F. Grusdt and J. C. Halimeh, *Disorder-free localization with Stark gauge protection*, *Phys. Rev. B* **106** (2022) 174305 [[2203.01338](#)].
- [115] J. C. Halimeh, L. Barbiero, P. Hauke, F. Grusdt and A. Bohrdt, *Robust quantum many-body scars in lattice gauge theories*, *Quantum* **7** (2023) 1004 [[2203.08828](#)].
- [116] D. J. Luitz and Y. B. Lev, *The ergodic side of the many-body localization transition*, *Ann. Phys.* **529** (2017) 1600350 [[1610.08993](#)].

- [117] S. W. Hawking, *Particle Creation by Black Holes*, *Commun. Math. Phys.* **43** (1975) 199.
- [118] S. W. Hawking, *Breakdown of Predictability in Gravitational Collapse*, *Phys. Rev. D* **14** (1976) 2460.
- [119] D. N. Page, *Is Black-Hole Evaporation Predictable?*, *Phys. Rev. Lett.* **44** (1980) 301.
- [120] D. N. Page, *Information in black hole radiation*, *Phys. Rev. Lett.* **71** (1993) 3743 [[hep-th/9306083](#)].
- [121] G. Dvali, M. Michel and S. Zell, *Finding Critical States of Enhanced Memory Capacity in Attractive Cold Bosons*, *EPJ Quant. Technol.* **6** (2019) 1 [[1805.10292](#)].
- [122] W. G. Unruh, *Experimental black hole evaporation*, *Phys. Rev. Lett.* **46** (1981) 1351.
- [123] W. G. Unruh, *Sonic analog of black holes and the effects of high frequencies on black hole evaporation*, *Phys. Rev. D* **51** (1995) 2827 [[gr-qc/9409008](#)].
- [124] M. Visser, *Acoustic black holes: Horizons, ergospheres, and Hawking radiation*, *Class. Quant. Grav.* **15** (1998) 1767 [[gr-qc/9712010](#)].
- [125] L. J. Garay, J. R. Anglin, J. I. Cirac and P. Zoller, *Sonic black holes in dilute Bose-Einstein condensates*, *Phys. Rev. A* **63** (2001) 023611 [[gr-qc/0005131](#)].
- [126] C. Barcelo, S. Liberati and M. Visser, *Towards the observation of Hawking radiation in Bose-Einstein condensates*, *Int. J. Mod. Phys. A* **18** (2003) 3735 [[gr-qc/0110036](#)].
- [127] C. Barcelo, S. Liberati and M. Visser, *Analogue gravity*, *Living Rev. Rel.* **8** (2005) 12 [[gr-qc/0505065](#)].
- [128] M. J. Jacquet, S. Weinfurter and F. König, *The next generation of analogue gravity experiments*, *Phil. Trans. Roy. Soc. Lond. A* **378** (2020) 20190239 [[2005.04027](#)].
- [129] J. D. Bekenstein, *Black holes and entropy*, *Phys. Rev. D* **7** (1973) 2333.
- [130] G. W. Gibbons and S. W. Hawking, *Cosmological Event Horizons, Thermodynamics, and Particle Creation*, *Phys. Rev. D* **15** (1977) 2738.
- [131] E. Mottola, *Particle Creation in de Sitter Space*, *Phys. Rev. D* **31** (1985) 754.
- [132] L. H. Ford, *Quantum Instability of De Sitter Space-time*, *Phys. Rev. D* **31** (1985) 710.
- [133] E. Mottola, *Thermodynamic instability of de Sitter space*, *Phys. Rev. D* **33** (1986) 1616.
- [134] I. Antoniadis, J. Iliopoulos and T. N. Tomaras, *Quantum Instability of De Sitter Space*, *Phys. Rev. Lett.* **56** (1986) 1319.
- [135] U. H. Danielsson, D. Domert and M. E. Olsson, *Miracles and complementarity in de Sitter space*, *Phys. Rev. D* **68** (2003) 083508 [[hep-th/0210198](#)].
- [136] N. Goheer, M. Kleban and L. Susskind, *The Trouble with de Sitter space*, *JHEP* **07** (2003) 056 [[hep-th/0212209](#)].
- [137] T. Banks and W. Fischler, *An Upper bound on the number of e-foldings*, [astro-ph/0307459](#).
- [138] N. Arkani-Hamed, S. Dubovsky, A. Nicolis, E. Trincherini and G. Villadoro, *A Measure of de Sitter entropy and eternal inflation*, *JHEP* **05** (2007) 055 [[0704.1814](#)].
- [139] P. O. Fedichev and U. R. Fischer, *'Cosmological' quasiparticle production in harmonically trapped superfluid gases*, *Phys. Rev. A* **69** (2004) 033602 [[cond-mat/0303063](#)].

- [140] P. O. Fedichev and U. R. Fischer, *Gibbons-Hawking effect in the sonic de Sitter space-time of an expanding Bose-Einstein-condensed gas*, *Phys. Rev. Lett.* **91** (2003) 240407 [[cond-mat/0304342](#)].
- [141] C. Barcelo, S. Liberati and M. Visser, *Analog models for FRW cosmologies*, *Int. J. Mod. Phys. D* **12** (2003) 1641 [[gr-qc/0305061](#)].
- [142] S. E. C. Weinfurtner, *Analog model for an expanding universe*, *Gen. Rel. Grav.* **37** (2005) 1549 [[gr-qc/0404063](#)].
- [143] U. R. Fischer and R. Schutzhold, *Quantum simulation of cosmic inflation in two-component Bose-Einstein condensates*, *Phys. Rev. A* **70** (2004) 063615 [[cond-mat/0406470](#)].
- [144] M. Uhlmann, Y. Xu and R. Schutzhold, *Aspects of cosmic inflation in expanding Bose-Einstein condensates*, *New J. Phys.* **7** (2005) 248 [[quant-ph/0509063](#)].
- [145] L. Berezhiani, *On Corpuscular Theory of Inflation*, *Eur. Phys. J. C* **77** (2017) 106 [[1610.08433](#)].
- [146] G. Dvali, *S-Matrix and Anomaly of de Sitter*, *Symmetry* **13** (2020) 3 [[2012.02133](#)].
- [147] L. Berezhiani, G. Dvali and O. Sakhelashvili, *de Sitter space as a BRST invariant coherent state of gravitons*, *Phys. Rev. D* **105** (2022) 025022 [[2111.12022](#)].
- [148] G. Dvali and L. Eisemann, *Perturbative understanding of nonperturbative processes and quantumization versus classicalization*, *Phys. Rev. D* **106** (2022) 125019 [[2211.02618](#)].
- [149] L. D. Carr, C. W. Clark and W. P. Reinhardt, *Stationary solutions of the one-dimensional nonlinear schrödinger equation. ii. case of attractive nonlinearity*, *Phys. Rev. A* **62** (2000) 063611.
- [150] N. N. Bogolyubov, *On the theory of superfluidity*, *J. Phys. (USSR)* **11** (1947) 23.
- [151] P.-G. de Gennes, *Superconductivity Of Metals And Alloys*. CRC Press, 1999.
- [152] G. Dvali, *Area law microstate entropy from criticality and spherical symmetry*, *Phys. Rev. D* **97** (2018) 105005 [[1712.02233](#)].
- [153] G. Dvali, *Black Holes as Brains: Neural Networks with Area Law Entropy*, *Fortsch. Phys.* **66** (2018) 1800007 [[1801.03918](#)].
- [154] G. Dvali, *Quantum Gravity in Species Regime*, [2103.15668](#).
- [155] G. Dvali, *Area Law Saturation of Entropy Bound from Perturbative Unitarity in Renormalizable Theories*, *Fortsch. Phys.* **69** (2021) 2000090 [[1906.03530](#)].
- [156] G. Dvali, *Unitarity Entropy Bound: Solitons and Instantons*, *Fortsch. Phys.* **69** (2021) 2000091 [[1907.07332](#)].
- [157] G. Dvali, *Entropy Bound and Unitarity of Scattering Amplitudes*, *JHEP* **03** (2021) 126 [[2003.05546](#)].
- [158] G. Dvali and O. Sakhelashvili, *Black-hole-like saturons in Gross-Neveu*, *Phys. Rev. D* **105** (2022) 065014 [[2111.03620](#)].
- [159] G. Dvali, O. Kaikov and J. S. V. Bermúdez, *How special are black holes? Correspondence with objects saturating unitarity bounds in generic theories*, *Phys. Rev. D* **105** (2022) 056013 [[2112.00551](#)].

- [160] M. Michel and S. Zell, *Numerical data for "The Timescales of Quantum Breaking"*, [Zenodo dataset:10.5281/zenodo.8039017](https://zenodo.org/record/8039017) .
- [161] M. Michel and S. Zell, *QuantumBreaking-TimeScales*, <https://github.com/marco-michel/QuantumBreaking-TimeScales> .
- [162] M. Michel and S. Zell, *to appear*, .
- [163] T. Ohmi and K. Machida, *Bose-einstein condensation with internal degrees of freedom in alkali atom gases*, *J. Phys. Soc. Jpn* **67** (1998) 1822.
- [164] T.-L. Ho, *Spinor bose condensates in optical traps*, *Phys. Rev. Lett.* **81** (1998) 742.
- [165] Y. Kawaguchi and M. Ueda, *Spinor bose-einstein condensates*, *Phys. Rep.* **520** (2012) 253 [[1001.2072](https://arxiv.org/abs/1001.2072)].
- [166] M. Lu, N. Q. Burdick, S. H. Youn and B. L. Lev, *Strongly dipolar bose-einstein condensate of dysprosium*, *Phys. Rev. Lett.* **107** (2011) 190401.
- [167] K. Aikawa, A. Frisch, M. Mark, S. Baier, A. Rietzler, R. Grimm et al., *Bose-einstein condensation of erbium*, *Phys. Rev. Lett.* **108** (2012) 210401.
- [168] J. A. de Freitas Pacheco, E. Kiritsis, M. Lucca and J. Silk, *Quasiextremal primordial black holes are a viable dark matter candidate*, *Phys. Rev. D* **107** (2023) 123525 [[2301.13215](https://arxiv.org/abs/2301.13215)].
- [169] O. Lahav, A. Itah, A. Blumkin, C. Gordon and J. Steinhauer, *Realization of a sonic black hole analogue in a Bose-Einstein condensate*, *Phys. Rev. Lett.* **105** (2010) 240401 [[0906.1337](https://arxiv.org/abs/0906.1337)].
- [170] F. Belgiorno, S. L. Cacciatori, M. Clerici, V. Gorini, G. Ortenzi, L. Rizzi et al., *Hawking radiation from ultrashort laser pulse filaments*, *Phys. Rev. Lett.* **105** (2010) 203901 [[1009.4634](https://arxiv.org/abs/1009.4634)].
- [171] S. Weinfurter, E. W. Tedford, M. C. J. Penrice, W. G. Unruh and G. A. Lawrence, *Measurement of stimulated Hawking emission in an analogue system*, *Phys. Rev. Lett.* **106** (2011) 021302 [[1008.1911](https://arxiv.org/abs/1008.1911)].
- [172] S. Eckel, A. Kumar, T. Jacobson, I. B. Spielman and G. K. Campbell, *A rapidly expanding Bose-Einstein condensate: an expanding universe in the lab*, *Phys. Rev. X* **8** (2018) 021021 [[1710.05800](https://arxiv.org/abs/1710.05800)].
- [173] Z. Fifer, T. Torres, S. Erne, A. Avgoustidis, R. J. A. Hill and S. Weinfurter, *Analog cosmology with two-fluid systems in a strong gradient magnetic field*, *Phys. Rev. E* **99** (2019) 031101 [[1801.05843](https://arxiv.org/abs/1801.05843)].
- [174] M. Wittmer, F. Hakelberg, P. Kiefer, J.-P. Schröder, C. Fey, R. Schützhold et al., *Phonon Pair Creation by Inflating Quantum Fluctuations in an Ion Trap*, *Phys. Rev. Lett.* **123** (2019) 180502 [[1903.05523](https://arxiv.org/abs/1903.05523)].
- [175] J. Steinhauer, M. Abuzarli, T. Aladjidi, T. Bienaimé, C. Piekarski, W. Liu et al., *Analogous cosmological particle creation in an ultracold quantum fluid of light*, *Nature Commun.* **13** (2022) 2890 [[2102.08279](https://arxiv.org/abs/2102.08279)].
- [176] C. Viermann et al., *Quantum field simulator for dynamics in curved spacetime*, *Nature* **611** (2022) 260 [[2202.10399](https://arxiv.org/abs/2202.10399)].
- [177] J. Hu, L. Feng, Z. Zhang and C. Chin, *Quantum simulation of Unruh radiation*, *Nature Phys.* **15** (2019) 785 [[1807.07504](https://arxiv.org/abs/1807.07504)].

- [178] G. Dvali, *Classicalization Clearly: Quantum Transition into States of Maximal Memory Storage Capacity*, [1804.06154](#).
- [179] T. Tao, *Topics in Random Matrix Theory*, Graduate studies in mathematics, Vol. 132. American Mathematical Society, 2012.